

CIAMTIS

U.S. DOT Region 3 University Transportation Center

Use of Machine Learning to Predict Long-Term Skid Resistant of Concrete Pavement

November 30, 2021

Prepared by:

F. Rajabipour and J. Yoon

**Department of Civil and Environmental Engineering
The Pennsylvania State University**

r3utc.psu.edu



PennState
College of Engineering

**LARSON
TRANSPORTATION
INSTITUTE**

DISCLAIMER

The contents of this report reflect the views of the authors, who are responsible for the facts and the accuracy of the information presented herein. This document is disseminated in the interest of information exchange. The report is funded, partially or entirely, by a grant from the U.S. Department of Transportation's University Transportation Centers Program. However, the U.S. Government assumes no liability for the contents or use thereof.

1. Report No. CIAM-COR-R28	2. Government Accession No.	3. Recipient's Catalog No.	
4. Title and Subtitle Use of Machine Learning to Predict Long-Term Skid Resistant of Concrete Pavement		5. Report Date November 30, 2021	
		6. Performing Organization Code	
7. Author(s) Farshad Rajabipour orcid.org/0000-0002-6616-0539 and Jinyoung Yoon		8. Performing Organization Report No. LTI 2022-03	
9. Performing Organization Name and Address The Pennsylvania State University Department of Civil and Environmental Engineering 212 Sackett Building, University Park, PA 16802, USA		10. Work Unit No. (TRAI5)	
		11. Contract or Grant No. 69A3551847103	
12. Sponsoring Agency Name and Address U.S. Department of Transportation Research and Innovative Technology Administration 3rd Fl, East Bldg E33-461 1200 New Jersey Ave, SE Washington, DC 20590		13. Type of Report and Period Covered Final Report 05/01/2020 – 02/28/2021	
		14. Sponsoring Agency Code	
15. Supplementary Notes Work funded through The Pennsylvania State University through the University Transportation Center Grant Agreement, Grant No. 69A3551847103.			
16. Abstract An adequate level of skid resistance over the service life of concrete pavements is crucial for the safety of drivers, especially in wet weather. It has been known that frictional properties of concrete pavements are influenced by concrete mixture proportions, type/properties of aggregates, surface texturing, and degree of surface polishing. Several experimental studies have attempted to establish regression correlations between these factors with time-dependent frictional properties of concrete pavements. While these experiments are necessary, they are costly and labor-intensive. As such, the current project intends to use the datasets and body of information generated by these past studies to develop a robust prediction algorithm for frictional properties of concrete pavements using the power of machine learning. More specifically, artificial neural network (ANN) is employed to resolve highly complicated relationships between frictional properties of concrete pavements and the parameters that influence such properties (e.g., aggregate mineralogy, concrete mixture proportions, etc.). Both the time-dependent frictional properties and terminal friction values are investigated. This report also provides a broad literature review on the subject.			
17. Key Words Concrete pavements, machine learning, artificial neural network, skid resistance, safety		18. Distribution Statement No restrictions. This document is available from the National Technical Information Service, Springfield, VA 22161	
19. Security Classif. (of this report) Unclassified	20. Security Classif. (of this page) Unclassified	21. No. of Pages 50	22. Price

Table of Contents

1. Introduction	1
Research Background.....	1
Research Objectives.....	2
Literature Review	2
Pavement Frictional Properties	2
Measurement of Pavement Friction	7
Measurement of Pavement Texture	9
Accelerated Polishing Devices	11
Factors Influencing Pavement Friction and Texture.....	15
Artificial Neural Network.....	16
2. Methodology	18
Outline	18
Establishment of Database for the ANN Model.....	19
3. Findings.....	27
Determination of ANN Structure	27
ANN-Based Prediction Results	29
Prediction of Friction and Texture Using the ANN Model.....	29
Sensitivity Analysis	29
IFI Friction and Skid Number	30
Prediction of Long-Term Skid Number	31
Estimation of Terminal Friction.....	35
4. Conclusions	39
References	40

List of Figures

Figure 1. Schematic diagram of force for a rotating wheel [1].....	2
Figure 2. Mechanisms of adhesion and hysteresis [1,25,27]	3
Figure 3. Illustration of various texture ranges that exist for a given pavement surface [6]	4
Figure 4. Relationship between texture and characteristics of the pavement surface [28].....	4
Figure 5. Examples of (a) ground, (b) grooved, and (c) NGCS pavement [32,34]	6
Figure 6. Schematic diagram of diamond-ground/grooved concrete.....	6
Figure 7. Heads of (a) grinding, (b) grooving, and (c) NGCS [34]	7
Figure 8. Test methods for measuring pavement friction: (a) British pendulum test [35], (b) Dynamic friction test, and (c) Locked-wheel test [36].....	8
Figure 9. Test methods for measuring texture of pavement: (a) volumetric sand patch test [39], (b) circular track/texture meter [40], and (c) 3d laser scanning device mounted on vehicle [38]	10
Figure 10. Accelerated polishing machine: (a) British polishing wheel, (b) Michigan indoor wear track [45], (c) North Carolina State University wear and polishing machine, (d) three-wheel polishing device [46], (e) accelerated wheel tracking chamber [3], and (f) model mobile load simulator [6]	12
Figure 11. Sample preparation for TWPD test: (a) concrete slab [51], (b) cylindrical asphalt concrete specimen with a testing ring [52], and (c) preparation of aggregate sample and holding this using square mold (MSMT 215).....	14
Figure 12 Schematic diagram of an ANN model [12].....	17
Figure 13. Outline of proposed ML-based prediction model for frictional properties of concrete pavements	18
Figure 14. DFT20 of plain concrete at 0–360k polishing (Dataset 1: PC1–9)	23
Figure 15. CTM of plain concrete at 0–360k polishing (Dataset 1: PC1–9)	23
Figure 16. DFT20 of ground/grooved concrete at 10k–160 k polishing(Dataset 2: GC1–9).....	24
Figure 17. CTM of ground/grooved concrete at 160k polishing (Dataset 2: GC1–9).....	24
Figure 18. DFT20 of ground/grooved concrete at 0k–160 k polishing (Dataset 3: GC10–14)	25
Figure 19. CTM of ground/grooved concrete at 0–160k polishing (Dataset 3: GC10–14).....	25
Figure 20. Linear relationship between DFT 60 and DFT20.....	26
Figure 21. Prediction results using ANN: (a) DFT20 and (b) CTM.....	29
Figure 22. Contribution of input parameters on DFT20 and CTM (Grind- or Groove- S, G, and D means spacer, gap, and depth, respectively)	30
Figure 23. Prediction results for the skid number at 65 km/h (SN65s)	32
Figure 24. Predicted long-term frictional properties of plain concrete pavement	33
Figure 25. Predicted long-term frictional properties of ground/grooved concrete pavement.....	34
Figure 26. Life cycle of pavement depending on a degree of polishing [66]	36
Figure 27. Determination of polishing cycles in a plateau of normalized STD of GC14-4's SN65s to identify terminal SN65s	37

List of Tables

Table 1. Summary of literature datasets used in this study.....	20
Table 2. Characteristics of grinding and grooving applied for concrete pavement	21
Table 3. Mixture proportions for plain concrete [6,29,51]	22
Table 4. Inputs and outputs used for the ANN model	26
Table 5. Evaluation of prediction error for DFT20 depending on the numbers of hidden layers and hidden neurons	28
Table 6. Evaluation of prediction error for CTM depending on the numbers of hidden layers and hidden neurons	28
Table 7. MAE and RMSE of DFT20 and CTM.....	29
Table 8. Coefficients for power-law regression model.....	32
Table 9. The ANN-based estimation of terminal friction of plain and ground and grooved concrete.....	38

CHAPTER 1

Introduction

RESEARCH BACKGROUND

The safety of the vehicular passengers, particularly in wet weather, is dependent upon friction characteristics between the vehicle tires and the pavement surface. While new concrete pavements often demonstrate adequate friction immediately after construction (e.g., by means of surface tinning, diamond grinding, and/or grooving), over time the pavement surface is polished by repeated tire abrasion, resulting in loss of skid resistance and potential for compromised safety to travelers.

The friction of concrete pavements has been described to depend upon macro- and micro-texture. Macro-texture refers to roughness on the centimeter scale. It reduces the potential for separation of the tire and pavement surface due to hydroplaning and is known to influence friction at higher travel speeds. On the other hand, micro-texture is at a smaller scale (mm and μm) and predominates the skid resistance behavior at both lower and higher speeds [1]. Limited past research is available on factors that control the resistance of concrete pavements against loss of friction and texture. It is generally known that polish resistance depends on the mineralogy and properties of the aggregates as well as the composition of the cement binder. In addition, surface preparation of concrete, including the type and quality of finishing and curing, is important. Therefore, to understand the loss of frictional properties of concrete pavements as a function of time, many factors, such as resistance of aggregates to polishing, pavement surface texturing technique and characteristics, and concrete mixture proportions, should be considered [2,3].

Recently, several studies have attempted to establish regression correlations linking these input factors (concrete mix design, aggregate polishability, and pavement surface treatment) with the time-dependent texture and frictional properties of concrete pavements [4–7]. These studies have relied on accelerated pavement polishing methods, such as the Wehner-Schulze device, the three-wheel polishing device, and model mobile load simulator (MMLS-3); and measuring the texture and friction of the tested pavements as a function of the number of polishing cycles. This approach is necessary to collect a sufficient body of experimental data. However, these experiments are costly and labor-intensive and may have poor generality, meaning that additional testing may be required if different materials or mixture proportions are used. However, these past studies have generated a body of experimental data that can be used for the development of more robust prediction algorithms such as via machine learning.

Machine learning (ML) can be employed to resolve highly complicated relationships between inputs (concrete mixture proportions, ingredient material properties, surface treatment, degree of polishing) and output variables (friction and texture) by improving the generality of the prediction model. ML algorithms that have become available in recent years provide a means for developing predictive models that can explain an inherent nonlinear relationship between inputs and outputs. The artificial neural network (ANN), which is one of the most powerful ML algorithms, has been successfully used in the field of civil engineering, including such applications as damage assessment [8–10], prediction model for concrete mechanical properties [11–13], and concrete mixture optimization [14,15]. In a concrete/asphalt pavement study, the ANN-based model showed good performance for evaluating surface roughness [16,17], deterioration [18,19], or lifecycle performance [20]. The success of these past studies suggests that ANN models may be well suited for predicting the time-dependent friction and texture of concrete pavements by using the available experimental data from accelerated pavement polishing studies.

RESEARCH OBJECTIVES

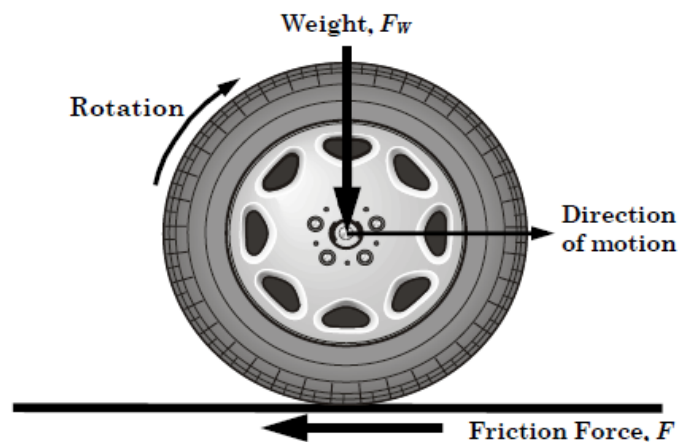
The objective of this study is to develop an ANN-based model for predicting the long-term friction and texture of plain and ground/grooved concrete pavements. First, a database is constructed using the available data from the literature. This database contains more than 200 data points of concrete mixture proportions, aggregate types, polishing resistance, pavement surface friction measured using the Dynamic Friction Tester, DFT (ASTM E1911-19), and pavement surface texture measured using the Circular Track Meter, CTM (ASTM E2157-15) [21,22]. The latter two parameters are inputted in the model as a function of the number of the accelerated polishing cycles. These prediction results are used for determining the international friction index (IFI) parameters and equivalent skid number measured by locked-wheel trailer test (ASTM E274-15) [23]. With the use of this equivalent skid number, the ANN model is extrapolated to investigate the long-term frictional properties of pavements beyond the accelerated testing ranges provided in the literature. Based on the predicted long-term friction results, the terminal friction of concrete pavement is estimated using the normalized standard deviation-based method. It is expected that the application of this ANN-based model enables designers and contractors to construct high-quality concrete pavements with long-term friction retention.

LITERATURE REVIEW

This section mainly focuses on a literature review of pavement friction and texture and the ANN model. A basic knowledge of pavement friction and texture is first introduced. Characteristics of surface texturing techniques (e.g., grinding and grooving), which improve the frictional properties of pavements, are also provided. Additionally, various testing methods and devices for measuring pavement friction and texture are introduced, as well as equipment for accelerated polishing, which simulate wearing of pavements. Lastly, a literature review of ANN is presented.

Pavement Frictional Properties

Pavement friction (also known as “skid resistance”) is the resistive force resulting from the interaction between the vehicle tire and the pavement surface, as shown in **Figure 1**. The resistive force is generally characterized by the non-dimensional friction coefficient (μ). The friction coefficient is the ratio of tangential force (F) at the contact area to the normal force on the tire (F_w) [1].



In a tire-pavement contact area, the friction is influenced by the complex interaction of two main mechanisms of adhesion and hysteresis (see **Figure 2**). Adhesive force is one of the components influencing

tire-pavement friction in dry weather and at low-speed. This adhesion friction is generated by the tire rubber-pavement interaction at a micro-level (micro-texture), such as fine aggregate particles, when the tire is pressed into pavement surface [24]. Hysteresis force is developed by the bulk deformation of tire rubber when it contacts with pavement surface [25]. During the tire relaxation, some of the stored energy is lost in the form of heat (hysteresis), while the remaining energy is recovered in the form of mechanical energy. This hysteresis force is highly influenced by the macro-texture of pavement. These two components of skid resistance are related to the key properties of road pavement surfaces [1,26].

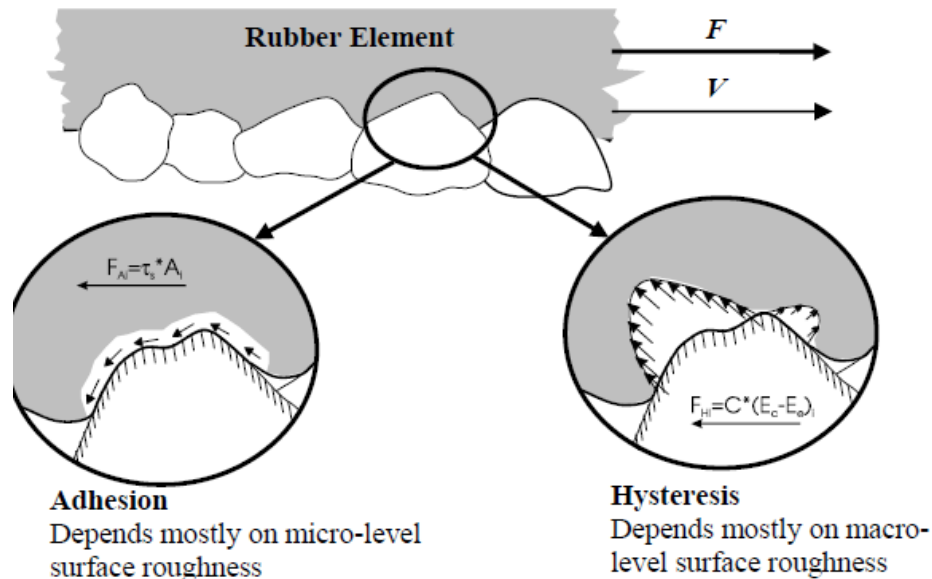


Figure 2. Mechanisms of adhesion and hysteresis [1,25,27].

Texture on pavement means the irregularities of pavement surface: “deviations of the pavement surface from a true planar surface” [28,29]. The deviations can be identified at different levels of wavelength (λ) and amplitude (A) of its components. It should be noted that the wavelength means the length between physically repeating parts (pavement surface features) [1]. According to the Permanent International Association of Road Congress (PIARC), the textures can be categorized as follows (see **Figure 3**):

- Micro-texture ($\lambda < 0.5$ mm, $A = 1-500$ μ m): Surface roughness at the microscopic level.
- Macro-texture ($\lambda = 0.5-50$ mm, $A = 0.1-20$ mm): Surface roughness quality defined by the mixture properties, and the surface treatment method of finishing/texturing (e.g., burlap drag, tinning, diamond grinding, grooving).
- Mega-texture ($\lambda = 50-500$ mm, $A = 0.1-50$ mm): Texture with wavelengths in the same order of magnitude as the pavement-tire interface. It is largely defined by the distress or defects on the pavement surface (e.g., potholes).

The properties of pavement texture can be influenced by aggregate size and gradation, aggregate morphology, mix proportions, surface texture dimensions (e.g., spacing between grooves), and texture orientation. However, it is well established that micro-texture is highly dependent on the roughness of individual coarse and fine aggregate particles, whereas the large irregularities of a road surface (coarse-scale) influence the macro-texture of pavement [30].

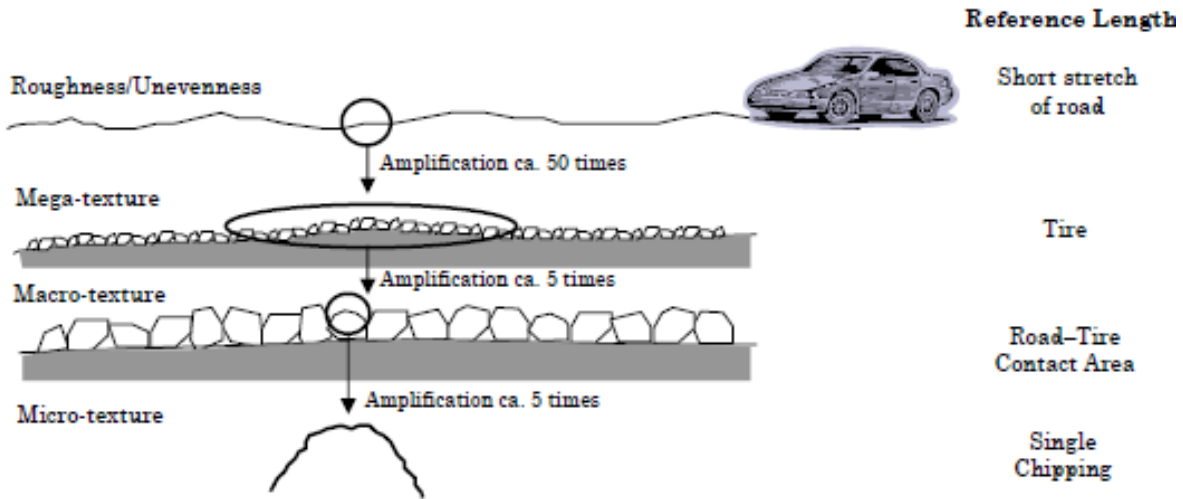


Figure 3. Illustration of various texture ranges that exist for a given pavement surface [6].

It has been widely known that various interactions between tire and pavement, such as dry or wet weather friction, tire wear, noise, and ride quality, are influenced by the degree of pavement texture (see **Figure 4**) [28]. As, the macro-texture of the pavement is a key parameter affecting the drainage capacity as well as the driving safety of wet pavements, the characterization of macro-texture is one of the important tasks to evaluate the frictional properties of pavements [31]. On the contrary, micro-texture of pavements influences the handling of vehicles at low speed or in dry weather.

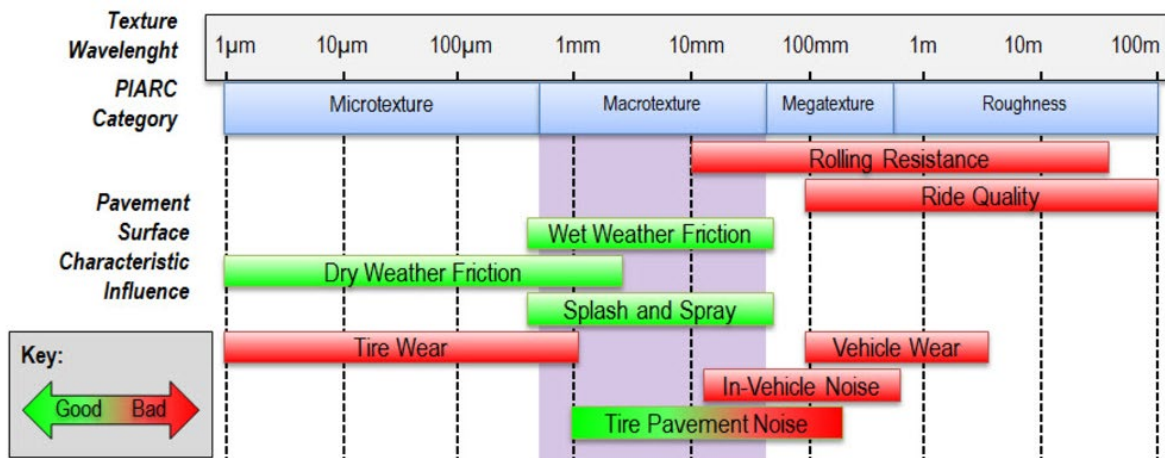


Figure 4. Relationship between texture and characteristics of the pavement surface [28].

In recent years, pavement surface texturing techniques have been applied to improve the ride quality and reduce pavement-tire noise. Diamond grinding and grooving is one of the commonly used surface treatment methods in new construction and in rehabilitation of existing pavements (see **Figure 5**). Using diamond grinding, the surface irregularities of a road caused by construction work or traffic loading over time can be removed [29]. Accordingly, the smoothness and surface friction of pavement can be improved or restored. The characteristics (texture) of the diamond ground surface depend on the cutting depth and spacing between the grinding blades, as shown in **Figures 6** and **7**. Diamond grooving creates parallel channels on the pavement surface to improve water drainage and to reduce the hydroplaning potential [29]. Two types of longitudinal and transverse grooving are commonly used. Longitudinal

grooving improves lateral friction and is generally used for decreasing the hydroplaning potential and improvement of curve tracking [32]. Transverse grooving provides better water drainage, but noise could be increased [32]. A schematic diagram of diamond ground and grooved pavement is provided in **Figure 6**. One of the texturing methods—Next Generation Concrete Surface (NGCS), developed at Purdue University—has also been implemented due to its advantages of reducing road noise as well as improvement of macrotexture. As can be seen in **Figure 5 (c)**, texture of NGCS is very similar to ground/grooved pavement, but NGCS cuts deeper grooves (1/8 in. or deeper) at a wider spacing interval (around 1/2 in.) [32]. This can be achieved by using different types of diamond blades, as shown in **Figure 7**. It has been reported that the application of NGCS on pavement is helpful for reducing tire-pavement noise as well as improving frictional performance [33]. Even though various advantages of grinding/grooving have been introduced, it should be noted that the long-lived frictional properties of ground/grooved pavement can only be achieved with the use of hard and durable aggregates.

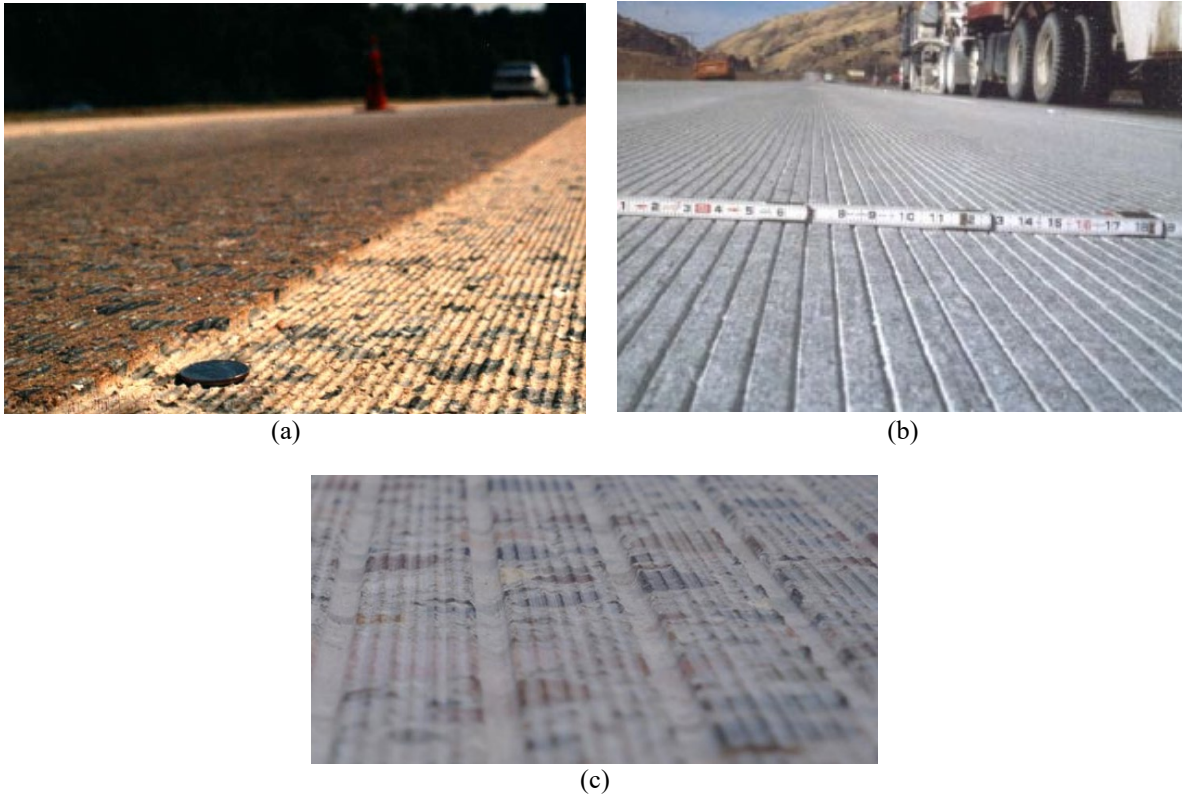


Figure 5. Examples of (a) ground, (b) grooved, and (c) NGCS pavement [32,34].

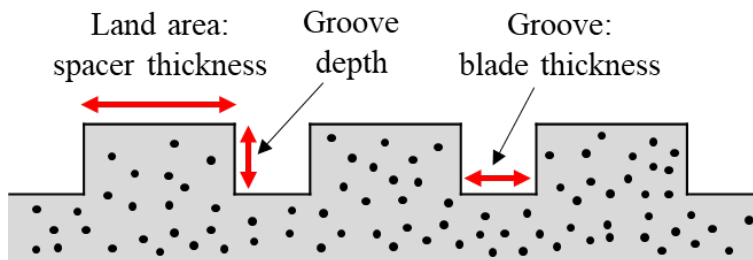


Figure 6. Schematic diagram of diamond-ground/grooved concrete.

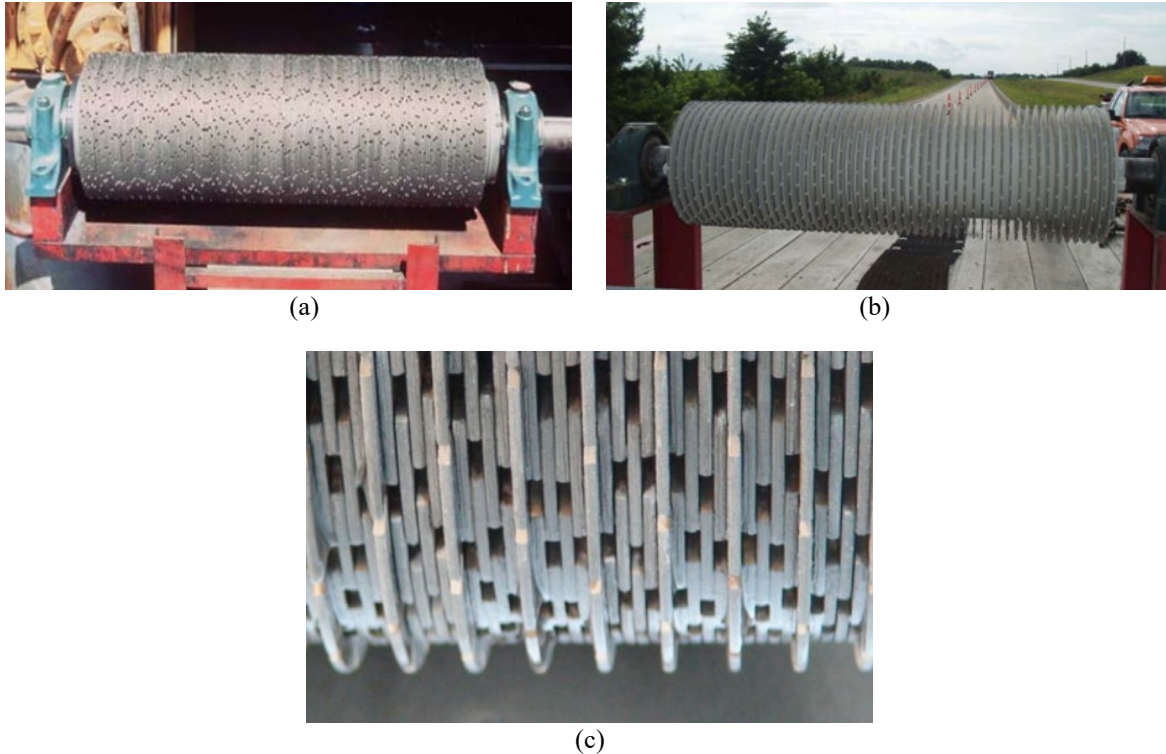


Figure 7. Heads of (a) grinding, (b) grooving, and (c) NGCS [34].

Measurement of Pavement Friction

A number of testing methods and devices have been developed to measure pavement friction. The British pendulum test (BPT, ASTM E303), dynamic friction test (DFT, ASTM E1911), and locked-wheel test (ASTM E274) have been extensively used, as shown in **Figure 8**.

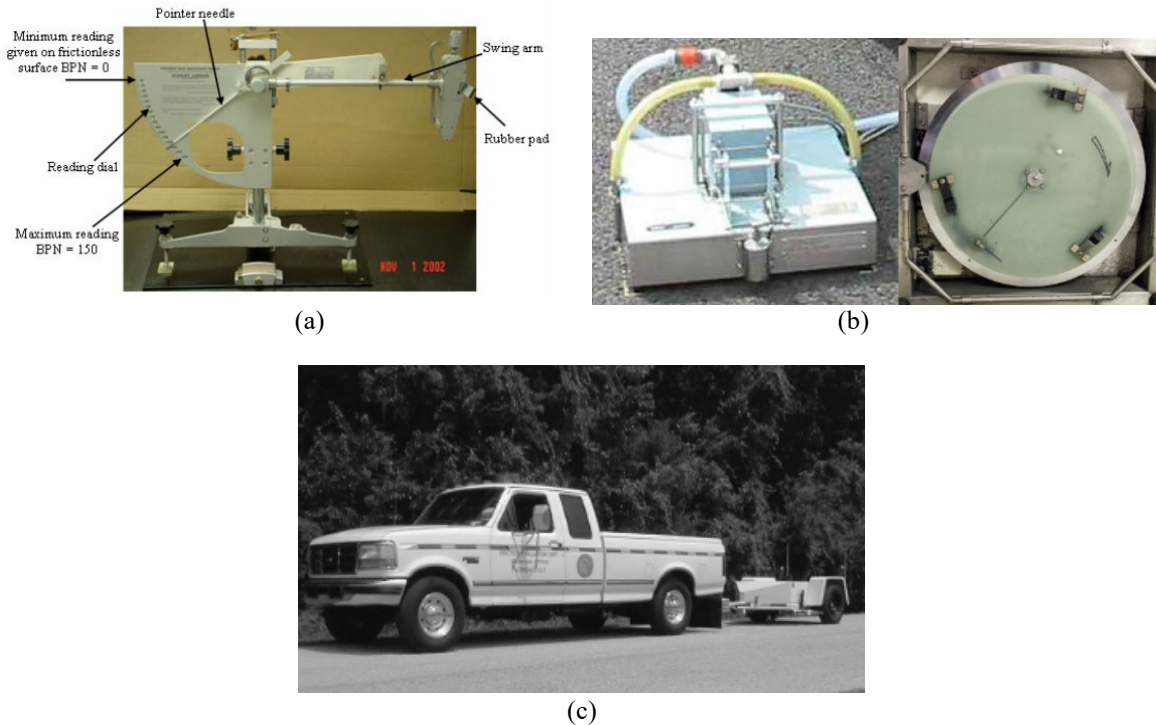


Figure 8. Test methods for measuring pavement friction: (a) British pendulum test [35], (b) dynamic friction test, and (c) locked-wheel test [36].

British pendulum test (BPT, ASTM E303) is one of the devices commonly used for measuring skid resistance (caused by macro-texture) of pavements in laboratory and field testing due to its good portability and simple testing method. This equipment consists of a tripod frame with a rubber slider on the head swing arm (pendulum). This device measures the loss of kinetic energy when the swing arm passes over the surface of tested samples [32]. As the loss of kinetic energy is converted to a frictional force, friction of normal and ground/grooved pavement can be determined. A high BPT number indicates a high skid resistance of the test sample. However, this testing method measures a relatively small testing area of road or concrete samples. Thus, the results from the British pendulum test may not represent the frictional properties of the road or testing sample. This testing device can also be used for analyzing frictional properties of coarse aggregates.

Likewise, the dynamic friction test (DFT, ASTM E1911) is a method extensively used for field and laboratory testing. Because this test is not highly influenced by the operator or presence of wind, its good repeatability and reproducibility have been reported [25]. DFT measures the coefficient of dynamic friction (caused by micro- and macro-texture) at different testing speeds from 0 to 80 km/h. DFT measures the torques applied on three small circular rotating pads. This torque is converted to a dynamic friction value. During the test, water is continuously supplied to the surface to simulate wet conditions.

The locked-wheel test (ASTM E274) is one of the commonly used methods in the United States for skid resistance of full-scale pavements. This test automatically records the frictional data using a locked-wheel trailer system [36]. The instrumented trailer with a locked-wheel system is towed behind the vehicle at a speed of 64 km/h or 96 km/h. During the test, water is sprayed in front of the test tire to simulate a wet pavement condition. Then the resistive drag force over a pavement surface under the constant speed is measured for 1–3 seconds. In this test, the locked-wheel trailer can be equipped with either a ribbed tire (ASTM E501) or a smooth tire (ASTM E524). The results of the locked-wheel test are reported as a friction number (FN) or skid number (SN), which can be expressed as:

$$FN(S) = 100 \times F/W$$

where S represents the velocity of the test tire, F represents the sum of all horizontal force applied to the tire, and W indicates the dynamic vertical load applied to the tire.

Measurement of Pavement Texture

For the measurement of pavement texture (see **Figure 9**), the conventionally used volumetric sand patch test (ASTM E965) and circular track meter test (ASTM E 2157) have been used. More recently, with the advancement of laser scanning technology, various types of pavement texture scanning devices using laser scanner have been developed [28,37,38].

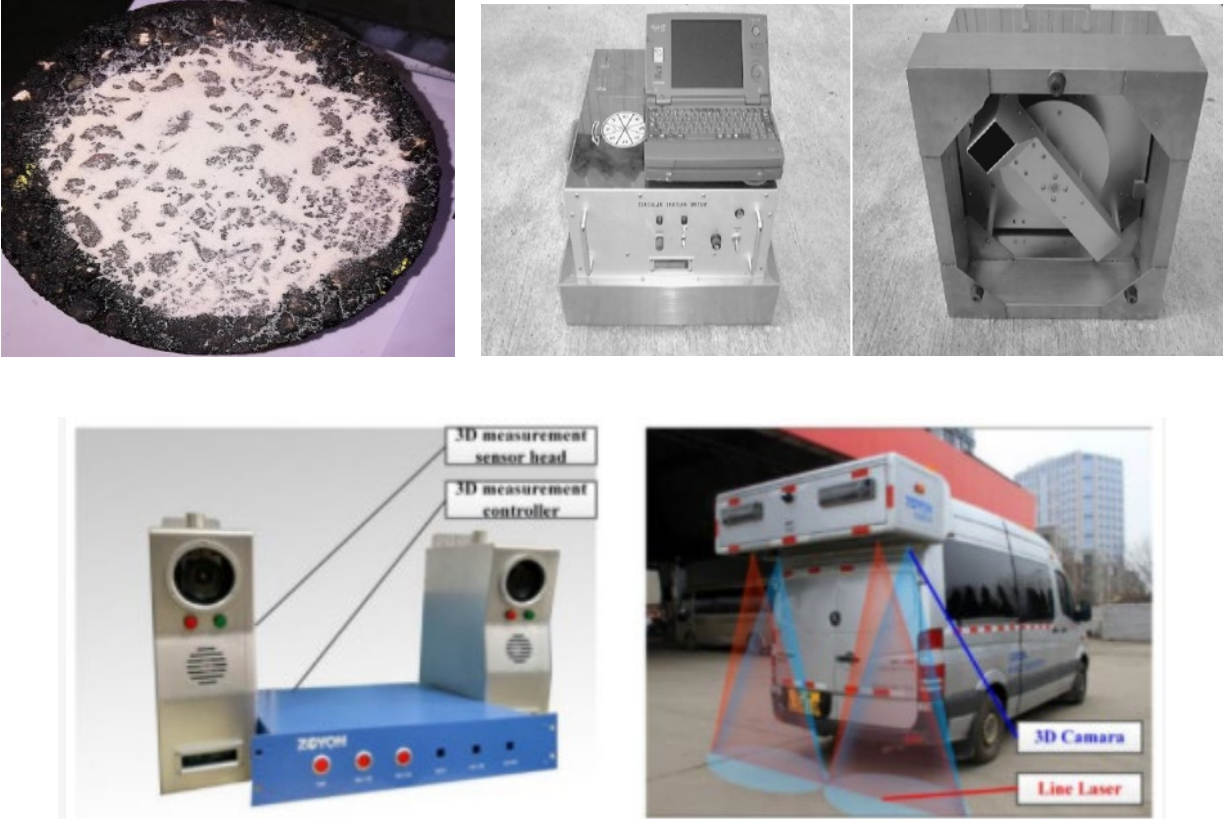


Figure 9. Test methods for measuring texture of pavement: (a) volumetric sand patch test [39], (b) circular track/texture meter [21], and (c) 3d laser scanning device mounted on vehicle [38].

The sand patch test (ASTM E965) is a volumetric technique measuring the macro texture of the pavement surface. This volumetric sand patch method is most commonly used to measure texture of pavement due to its simple and convenient testing procedure. This test consists of (1) spreading a material having uniform particles (e.g., sand or glass beads) of already known volume on a clean and dry pavement and then calculating the average depth of the macro-texture based on the area covered by the material. In specific, the diameter of the circle is measured on four axes and the average value is calculated. This value is then used to calculate the mean texture depth (MTD). According to ASTM E 965, the size of material (sand or glass bead) shall be graded to have a minimum of 90% by weight passing a No. 60 sieve and retained on a No. 80 sieve. The volume of material used for the test should be higher than 25 mL. Recently, glass beads are more preferred than sand because of the uniform spherical shape of glass beads [40].

The circular track meter (CTM) measures the mean profile depth (MPD) of a pavement macrotexture (ASTM E2157) utilizing a laser displacement sensor. The circular track meter can be applied in laboratory and field testing. The laser sensor is mounted on an arm that rotates in a circular path (284 mm in diameter), which is divided into eight segments for calculating each MPD. The average values of all eight segments indicate the mean profile depth of the testing sample. The laser spot size is 70 μm and the vertical resolution is 3 μm . The mean profile depth obtained from CTM has been shown to correlate well to the mean texture depth measured with the sand patch test [21,40,41]. Analysis of the circular track meter allows more detailed investigation of the texture to determine what is producing the texture and whether it is positive (raised), negative (grooved) or neutrally textured.

With significant advancements in laser technology, many kinds of laser scanning devices for the analysis of road surface condition have been developed. Because of the advantage of automated pavement data collection via 3D laser scanning system, laser scanning devices have been used for pavement crack

identification, macro-texture, skid resistance, and etc. [28,41–43]. The 3D laser scanning system mounted on the vehicle has effectively characterized the various pavement distresses, such as cracks, road markings, rutting, potholes, and textures [38,41].

Accelerated Polishing Devices

During the entire lifecycle of a pavement, the surface of pavement is continuously polished due to a traffic load. The polishing rate is typically dependent on the traffic load, which takes a long time. Thus, in order to simulate wearing and polishing of pavements, laboratory-scale accelerated polishing devices have been developed and used since research on skid resistance started in the 1960s (see **Figure 10**).

- British Polishing Wheel (ASTM D3319)
- Michigan Indoor Wear Track [44]
- North Carolina State University (NCSU) Wear and Polishing Machine (ASTM E660)
- Three-Wheel Polishing Device (TWPD) developed by the National Center for Asphalt Technology (NCAT) [45]
- Accelerated wheel tracking chamber [3]
- Model Mobile Load Simulator (MMLS-3) [6]

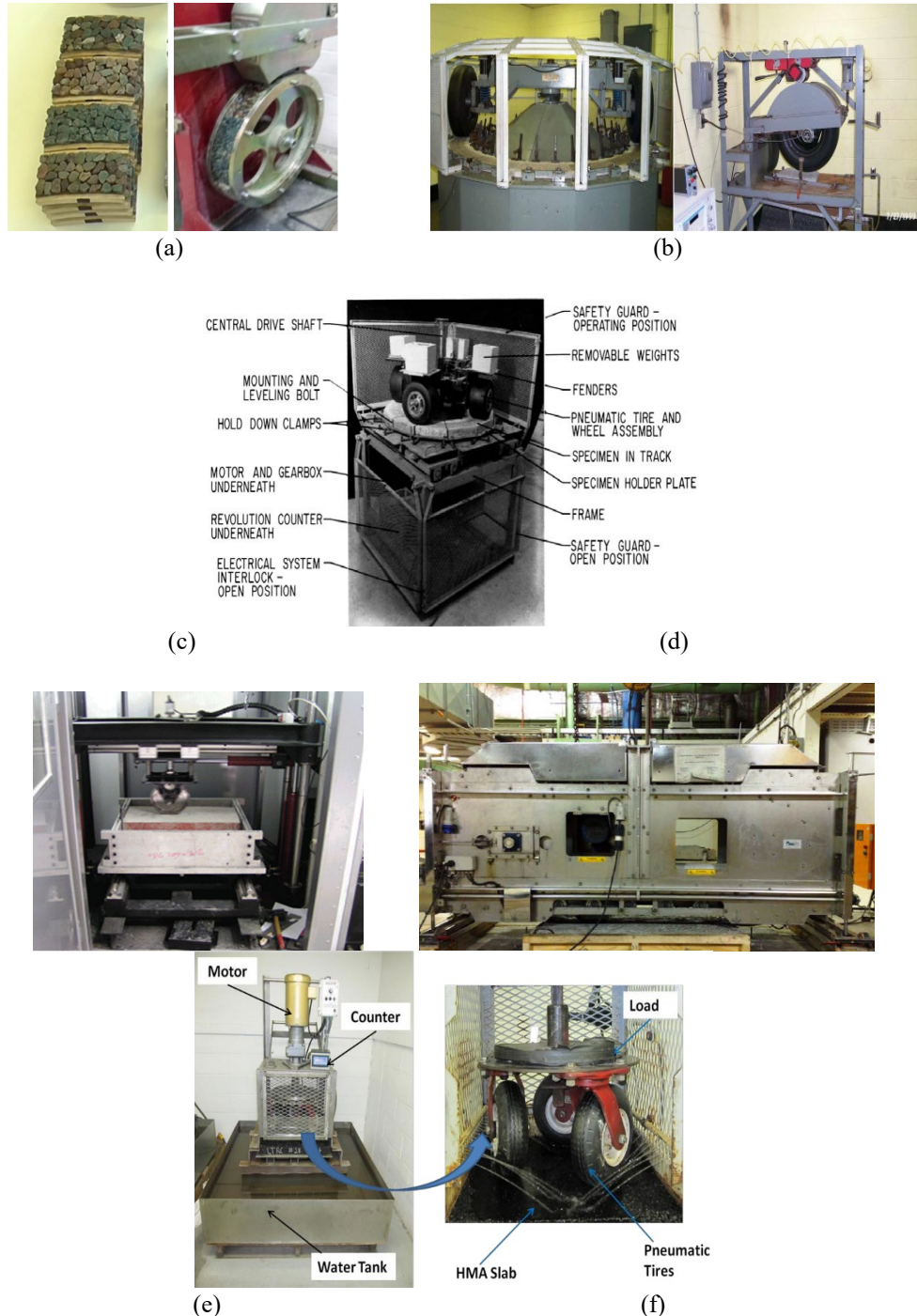


Figure 10. Accelerated polishing machine: (a) British polishing wheel, (b) Michigan indoor wear track [44], (c) North Carolina State University wear and polishing machine, (d) three-wheel polishing device [45], (e) accelerated wheel tracking chamber [3], and (f) model mobile load simulator [6].

Aggregate polishing is typically conducted using the British polishing wheel (also known as the British wheel) according to ASTM D3319. British polishing method is applicable for the curved aggregate specimens clamped around the periphery of the wheel assembly to form a continuous strip of aggregate particles [35,46]. The wheel is then rotated against a rubber-tire wheel that provides the polishing action.

The aggregate specimens are made with uniform sized coarse aggregate particles, which are mounted on the curved mold. In order to hold aggregate particles in the mold, bonding materials, such as epoxy resin, are poured. The polish-resistant frictional properties of aggregates can be measured using the British pendulum test according to ASTM E303.

The Michigan indoor wear track developed by the Michigan Department of Transportation can also be used for measuring the polish resistance of coarse aggregate samples [7,45,47,48]. The circular wear track of this device is very large, with a diameter of 2.1 m (7 ft) and simulates the rolling process of vehicles using a full-scale tire in accordance with ASTM E524. This device accommodates 16 trapezoidal specimens, which are made with coarse aggregate in the steel molds with binding materials. After the polishing process, aggregate friction tests are performed.

The North Carolina State University (NCSU) Wear and Polishing Machine was developed to evaluate changes in skid resistance of aggregates and paving mixtures after wear and polish [45]. As specified in ASTM E660, this circular track machine consists of four individually mounted and equally spaced wheels. Pneumatic tires used for this machine are nylon smooth tread tires having 138 kPa (20 psi) tire pressure with a wheel loading of 320 N. The diameter of the circular track is 914 mm (36 in) and a total of 12 equally spaced samples can be tested. After a few hours of polishing, the surface friction of each specimen is measured.

The Three Wheel Polishing Device (TWPD) developed by the National Center for Asphalt Technology (NCAT) is designed to simulate wear of the pavement surface [49]. This circular track polishing machine could polish the area of testing sample sufficiently large to accommodate the friction and texture measurements using a dynamic friction tester and circular texture meter, respectively. The NCAT polishing machine consists of a steel frame to which a vertical shaft is attached that holds an assembly of three small wheels rotating on a circular track 285 mm (11.2 in.) in diameter. In the test, a nominal 50.8–61.0 cm (20–24 in.) square slab has been used [49,50]. TWPD utilizes three pneumatic tires made of resin, hard rubber, polyurethane, or steel having a 20-cm (8-in) diameter [29]. During the polishing, water is sprayed to wash the abraded rubber particles on the surface of the testing specimen. The applied normal load on the wheel can be adjusted by adding/removing circular iron plates on the device's table. This TWPD has been used for assembly of cylindrical samples with a testing ring [51] and aggregate samples placed in a circular steel mold [52]. With the use of a testing ring, various pavement surface field cores can be tested (please see **Figure 11**). The drawback of this system lies in the fact that it can polish only a small circular area and texture and friction results may be influenced by the positioning of the respective devices onto the polished ring.

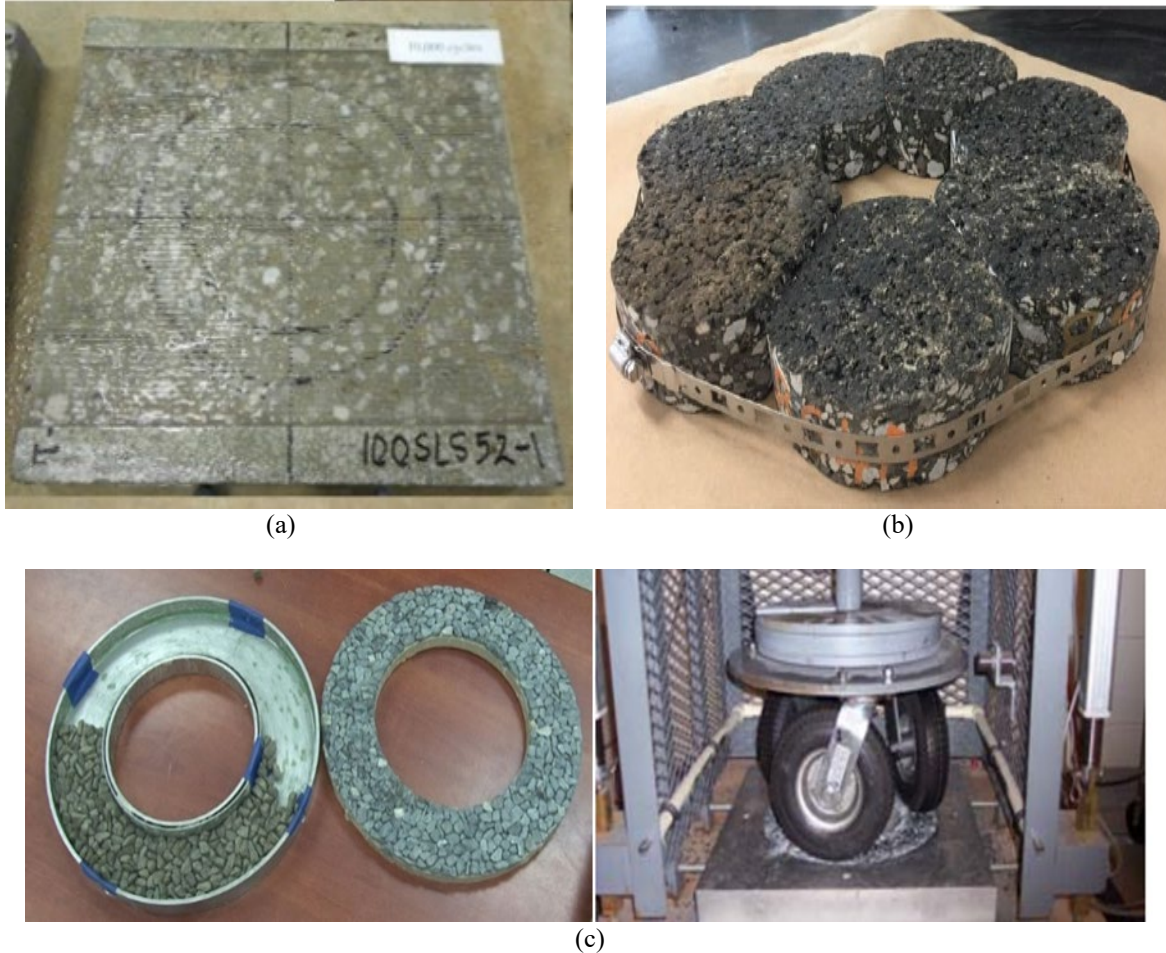


Figure 11. Sample preparation for TWPD test: (a) concrete slab [50], (b) cylindrical asphalt concrete specimen with a testing ring [51], and (c) preparation of aggregate sample and holding this using square mold (MSMT 215).

An accelerated wheel tracing chamber was used for the simulation of long-term skid resistance of $600 \times 300 \times 200$ mm concrete specimens [3]. A 60-kg steel wheel (50 mm in width) was repeatedly running on the concrete specimen. This simulation was conducted up to 100,000 cycles. This test is also applicable for aggregates according to ASTM D3319.

The Model Mobile Load Simulator also has been used for simulating traffic wearing [6,53]. It is commonly used to apply cycles to pavement markings, asphalt cement concrete pavements, and other highway materials to determine degradation of skid resistance. The MMLS-3 consists of four rotating axles equipped with a pneumatic tire (300 mm in diameter and up to 800 kPa pressure). The load level on each tire can vary from 2.1 kN (471 lbf) to 2.7 kN (606 lbf) through adjustment of the suspension system. This equipment is capable of applying up to 7,200 cycles per hour. The dimensions of the testing frame are 1.5 m (60 in.) by 0.3 m (12 in.) by 2.5 cm (about 1 in.) to 12.7 cm (5 in.) height and it can accommodate asphalt and concrete slab specimens.

Because many methods and devices evaluate skid resistance of pavement in their own way, the International Friction Index (IFI), a common scale for friction of pavement, is needed based on the correlation of different testing methods. Use of the IFI from a measurement of pavement macrotexture was explored by the Permanent International Association of Road Congress [54]. In 1992, PIARC conducted an international friction and texture harmonization study based on experimental research conducted at 54 different sites across the United States and Europe including 51 different measurement systems [1,29]. As a result of the PIARC experiment, IFI parameters of friction number (F60) and slip speed (S_p) are suggested

based on a mathematical model. For example, friction and texture values obtained from DFT and CTM can be used to calculate the IFI parameters. In accordance with ASTM E1960, the IFI parameters of $F60$ and S_P are first computed using the formulas provided in ASTM E1960:

$$S_P = 14.2 + 89.7MPD$$

$$F60 = A + B \times FR(S) \times e^{(S-60)/S_P}$$

where $A = 0.0082$ and $B = 0.732$, which are the coefficient of friction measured by DFT at 20 km/h (ASTM E1960), $FR(S)$ is the friction value measured at a speed S , and MPD is the mean profile depth measured by CTM.

$$F60 = 0.081 + 0.732DFT_{20}e^{-40/S_P}$$

After the IFI $F60$ and S_P are computed, the same formulas using different device constants can be used to compute the equivalent friction. To calculate the equivalent skid number (SN) measured by a locked-wheel test at different speed using a smooth tire (ASTM E524), the following equation can be used:

$$SN(S)_{Smooth} = \left(\frac{F60 - 0.045}{0.925} \times \frac{1}{e^{(S-60)/S_P}} \right) \times 100$$

Factors Influencing Pavement Friction and Texture

It was reported that several factors, such as polishing resistance of aggregates, pavement surface texturing techniques, and concrete mixture proportion, influence the friction and surface texture of a concrete pavement during its lifetime [2,3]. To ensure the adequate level of skid resistance of concrete pavement, aggregates having a high polishing resistance are more preferable. It has been known that polishing resistance of aggregates can vary depending on their mineralogy. For example, sandstone, granite, and gneiss have good initial and long-term skid resistance, while limestone and andesite have shown low polishing resistance [3]. The utilization of poor polishing-resistant aggregates is limited in wearing courses in the United States. For example, according to Pennsylvania Department of Transportation (PennDOT) Bulletin 14 [55], the use of aggregates in the courses is limited depending on the skid resistance level (SRL) of aggregates, which is based on types of aggregates: Excellent = sandstone, High = gneisses and granites, Good = siliceous limestone, Medium = dolomite, and Low = limestone. Coarse aggregates having excellent SRL can be applicable for high wearing courses (average daily traffic > 20,000). Similar specifications can be found in other state DOTs. In accordance with Louisiana Standard Specifications [56], the friction rating (FR) of aggregates is designated from I (high) to IV (low): FR I and II (e.g., sandstone) can be used for general purposes; FR III (e.g., gravel) is not allowed for courses with average daily traffic greater than 7,000; FR IV (e.g., limestone) is allowable if average daily traffic is less than 2,500. Even though these specifications are currently valid for asphalt concrete pavements, the skid resistance of coarse aggregates needs to be considered in the design of concrete pavement. With respect to modification of surface texturing of concrete pavement, diamond grinding and grooving methods have been applied to enhance smoothness and early-age friction of new pavements and to restore surface friction of in-service pavements [57]. Diamond grinding removes surface damage and irregularities using closely spaced saw blades. The advantages of diamond grinding are improvement of pavement smoothness, reduction of pavement-tire noise, and increased skid resistance. Grooving involves cutting the pavement with deeper cuts/grooves that serve as water drainage channels and help with prevention of hydroplaning in wet weather. The service life of surface treatments is also influenced by the type of aggregates. For example, in a ground and grooved concrete pavement that incorporates soft aggregates, the restored frictional properties will be short-lived if

the aggregates are exposed. In addition, mixture proportion of concrete pavement is also important due to its impact on strength and durability. Appropriate mixture design, with respect to water-to-cementitious materials ratio (w/cm), aggregate content, and types and dosages of pozzolans and chemical admixtures is developed to ensure concrete performance and to prevent durability problems during the pavement's intended design life.

Artificial Neural Network

Neural network-based models simulate the network of neurons in the human brain and are used to solve complicated problems. The basic structure of ANN consists of three types of layers: input, hidden, and output layers as shown in **Figure 12**. Depending on the number of hidden layers, the ANN can be classified into single- or multi-layer perceptron, which has multi-connected neurons. A neuron serves as a basic processing element, also known as a node. When neurons in the input layer receive an input, the weighted sums of the inputs are transferred to interconnected neurons in the next hidden layer and evaluated using activation functions. The weight and bias values can be updated and optimized in a minimization process of prediction error using the back-propagation algorithm. The backpropagation learning is repeated from the output layer to the input layer in each running step until there is no further decrease in the mean square error (MSE). After the training is completed with updated weight and bias, new inputs from the testing dataset are tested in the network to produce the corresponding outputs. The relationship between each hidden neuron ($h(x)$) and the input variables (x_i) can be expressed as [58]:

$$h(x) = f_h(b_i + \sum x_i w_i)$$

where f_h represents activation function and b_i and w_i are bias and weights, respectively. The sigmoidal function is commonly used as a nonlinear activation function in hidden layers. The equation of tangent sigmoidal function can be expressed as:

$$f_h(b_i + \sum x_i w_i) = \frac{2}{(1 + e^{-2(b_i + \sum x_i w_i)})} - 1$$

The predicted value, output (P), can be obtained:

$$P = f_0(b_j + \sum h_j w_j)$$

where activation function (f_0) is typically a linear activation function.

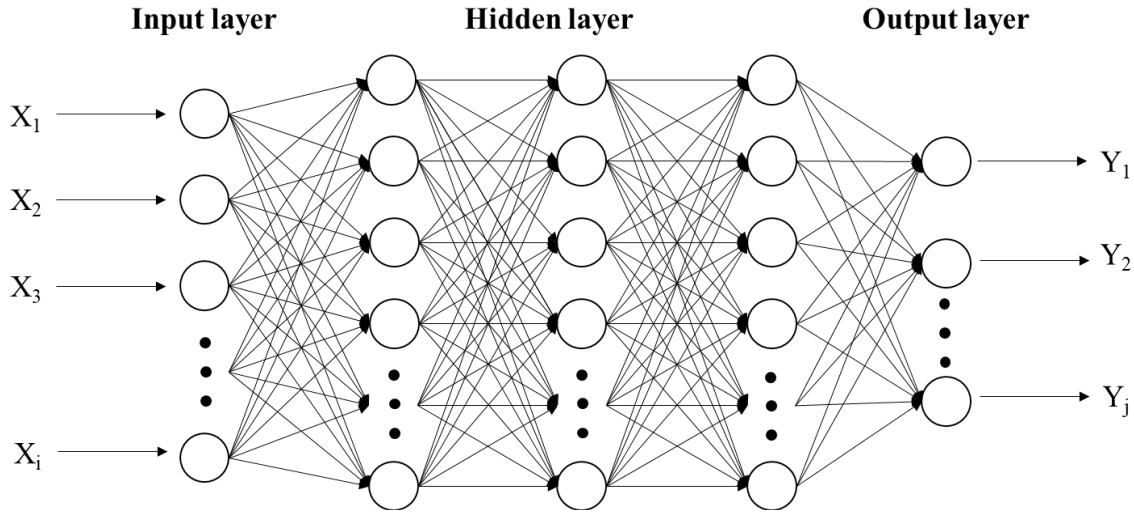


Figure 12. Schematic diagram of an ANN model [12].

To evaluate the reliability of the ANN model, various statistical metrics can be utilized. The mean square error, root mean square error (RMSE), mean absolute percentage error (MAE), and correlation coefficient (R) can be calculated as follows:

$$MSE = \frac{\sum_{i=1}^n (P_i - A_i)^2}{n}$$

$$RMSE = \sqrt{\frac{\sum_{i=1}^n (P_i - A_i)^2}{n}}$$

$$MAE = \frac{1}{n} \sum_{i=1}^n \left| \frac{P_i - A_i}{A_i} \right| \times 100\%$$

where n is the total number of specimens in the dataset, P_i is the predicted value, A_i is the target values, \bar{P}_i is the mean prediction, and \bar{A}_i is the mean target value.

CHAPTER 2

Methodology

OUTLINE

The ANN-based model for predicting frictional properties of concrete pavements was conducted as follows (see **Figure 13**): (1) data collection from literature; (2) evaluation of the prediction accuracies of the ANN model; and (3) calculation of the IFI friction and estimation of the long-term skid number beyond the testing ranges reported in the literature (i.e., extrapolation) as well as prediction of the terminal skid number.

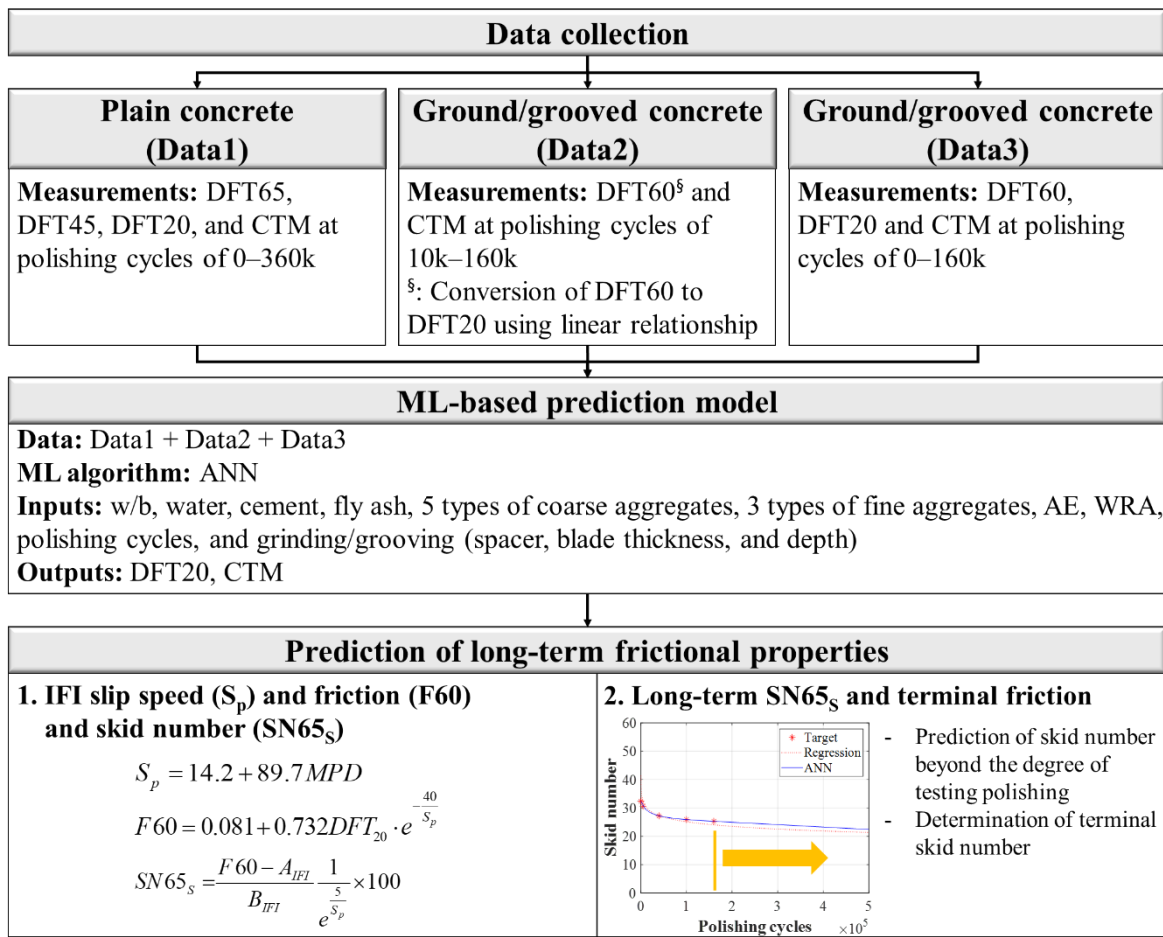


Figure 13. Outline of proposed ML-based prediction model for frictional properties of concrete pavements.

The development of the ANN model in this study was achieved as follows: (1) randomly splitting of the database into 80% of the data points for training and the remaining 20% for testing; (2) dividing the training dataset into 5 uniform-sized subsets (4 for training set and 1 for validation set); (3) training the

ANN model using the 4 training subsets and adopting a weight and bias when the model shows the highest accuracy for the validation set; (4) repeating step 3 five times and evaluating the model's performance using a different validation subset each time; and (5) evaluating final prediction accuracy for testing data with the ANN model that has the highest performance in step 4. It should be noted that the ANN model employed the Levenberg-Marquardt optimization method for adjusting the weight and bias for the network training. This algorithm is a combination of the steepest descent algorithm and the Gauss-newton algorithm [59]. The Levenberg-Marquardt algorithm is widely used due to its fast and stable performance compared to the conventionally used scaled conjugate gradient method.

ESTABLISHMENT OF DATABASE FOR THE ANN MODEL

Because accurate and reliable prediction using the ANN model is highly dependent on the size and quality of the data, establishment of the proper database is an important step in the development of the ANN model. The literature data were collected from three sources [6,29,50] that experimentally investigated the effect of aggregate types on the long-term frictional properties of “plain textured” and “ground and grooved” concrete slabs that were subjected to accelerated polishing in laboratories. These data were labeled as Dataset 1 (from [6]), Dataset 2 (from [50]), and Dataset 3 (from [29]). Depending on the composition of aggregates, the coarse and fine aggregates were categorized: limestone (LS), natural gravel (GV), granite (GR), dolomite (DM), natural sand (NS), and unknown (UKN). This is because aggregate mineralogy impacts its polishing resistance and the proposed aggregate classification can improve the generality of the ANN model.

The information of Datasets 1–3 used in this study are summarized in **Table 1**. Dataset 1 provides the results of long-term friction and texture measurements of plain surface concrete that was finished by hand trowel. A total of 9 concrete mixtures incorporating 5 coarse aggregates (3 limestone, 1 sandstone, and 1 granite) and 1 fine aggregate were used. The type of fine aggregate was not provided and was designated as unknown in the ANN model. Concrete mixtures contained 18% of fly ash and their w/cm were fixed at 0.40. Concrete slabs ($61.0 \times 66.0 \times 12.7 \text{ cm}^3$) were cast and cured at least 28 days. The MMLS03 accelerated polishing machine was used to simulate the wear and abrasion of the pavement caused by traffic load. The measurements of friction (via DFT at 20km/h) and texture (via CTM) were conducted after a specific number of polishing cycles in the range of 0 to 360K. A total of 90 data for each DFT20 and CTM were collected.

Table 1. Summary of literature datasets used in this study.

Label	Label	Type of Concrete Dataset 1 (plain concrete) [6]	Type of Concrete Dataset 2 (ground and grooved concrete) [50]	Type of Concrete Dataset 3 (ground and grooved concrete) [29]
Sample	Number of concrete mixtures	9	9	5
Sample	Slab dimensions	61.0 × 66.0 × 12.7 cm ³ (24 × 26 × 5 in ³)	50.8 × 50.8 × 8.9 cm ³ (20 × 20 × 3.5 in ³)	50.8 × 50.8 × 8.9 cm ³ (20 × 20 × 3.5 in ³)
Sample	Surface condition	Plain surface	5 different grinding/grooving	4 different grinding/grooving
Accelerated polishing equipment		Model Mobile Load Simulator (MMLS3)	Three-wheel polishing device (TWPD)	Three-wheel polishing device (TWPD)
Friction/texture tests	DFT	DFT20 at 0, 60K, 120K, 240K, and 360K polishing cycles	DFT60* at 10K, 40K, 100K, and 160K polishing cycles	DFT20 at 0, 5K, 40K, 100K, and 160K polishing cycles
Friction/texture tests	CTM	CTM at 0, 60K, 120K, 240K, and 360K polishing cycles	CTM at 160K	CTM at 0, 5K, 40K, 100K, and 160K polishing cycles

* DFT60 means DFT value at 60 km/h. This is converted to DFT20 using linear equation.

Datasets 2 and 3 were collected from the ground and grooved concrete slabs. In Dataset 2, a total of 9 concrete mixtures incorporating 3 coarse aggregates (1 granite and 2 limestones) and 1 siliceous river sand with $w/cm=0.45$ were tested. 96 concrete slabs ($50.8 \times 50.8 \times 8.9 \text{ cm}^3$) were cast. One plain surface concrete slab and 5 ground and grooved slabs with different surface treatments were made from each mixture. Details of the surface texture in terms of depth, spacer, and blade thickness used for grinding and grooving of these slabs are provided in **Table 2**. In Dataset 2, 363 data for DFT60 and 75 data for CTM were collected. Dataset 3 includes 5 concrete mixtures having $w/cm=0.42$. These concretes incorporated 4 different coarse aggregates (1 gravel, 1 dolomite, and 2 limestones) and 4 fine aggregates (2 siliceous natural sands and 2 limestone sands). Thirty concrete slabs ($50.8 \times 50.8 \times 8.9 \text{ cm}^3$) were cast and cured at least 28 days. Four different combinations of spacers, gaps (blade thickness), and depths of grinding and grooving were applied to each concrete mixture (Table 2). Dataset 3 has 100 data for each DFT20 and CTM. After the surface treatment, TWPD developed by NCAT was used for accelerated polishing of slabs in Datasets 2 and 3. These slabs were polished up to 160,000 cycles while DFT and CTM data were collected at a specific number of polishing cycles.

Table 2. Characteristics of grinding and grooving applied for concrete pavement.

Label	Label	Grinding (cm) Spacer	Grinding (cm) Blade Thickness	Grinding (cm) Depth	Grooving (cm) Spacer	Grooving (cm) Blade Thickness	Grooving (cm) Depth
Dataset 2 (GC1-9)	GC#-1	-	-	-	-	-	-
Dataset 2 (GC1-9)	GC#-2	0.279	0.318	0.635	-	-	-
Dataset 2 (GC1-9)	GC#-3	0.279	0.318	0.635	1.600	0.318	0.318
Dataset 2 (GC1-9)	GC#-4	0.330	0.318	0.635	-	-	-
Dataset 2 (GC1-9)	GC#-5	0.330	0.318	0.635	1.600	0.318	0.318
Dataset 2 (GC1-9)	GC#-6	0.102	0.318	0.076	1.143	0.318	0.318
Dataset 3 (GC10-14)	GC#-1	0.330	0.318	0.318	-	-	-
	GC#-2	0.279	0.318	0.318	-	-	-
	GC#-3	0.076	0.076	0.159	-	-	-
	GC#-4	0.076	0.076	0.159	1.588	0.318	0.318

More details on the mixture proportions of concretes in Datasets 1 through 3 are provided in **Table 3**. It should be noted that mixture proportion for every concrete in the units of kg/m^3 was calculated using specific gravity values for different concrete constituents when they were provided. Otherwise, the specific gravities were assumed as: 1.00 for water, 3.15 for portland cement, 2.50 for fly ash, 2.60 for coarse aggregate, 2.60 for fine aggregate, 1.18 for air-entraining agent (AE), and 1.35 for water-reducing agent (WR) [60].

Table 3. Mixture proportions (kg/m³) for plain concrete [6,29,50].

Label	w/cm	Water	Cement	Fly Ash	Coarse Agg.	Fine Agg.	Fine Agg.	Fine Agg.	AE	WR				
					LS	GV	SS	GR	DM	UKN	NS	LS		
PC1	0.40	147	312	55	1,198	0	0	0	0	704	0	0	0.62	0.95
PC2	0.40	147	312	55	838	0	359	0	0	704	0	0	0.62	0.95
PC3	0.40	147	312	55	359	0	838	0	0	704	0	0	0.62	0.95
PC4	0.40	147	312	55	838	359	0	0	0	704	0	0	0.62	0.95
PC5	0.40	147	312	55	359	838	0	0	0	704	0	0	0.62	0.95
PC6	0.40	147	312	55	570	0	0	0	0	1,331	0	0	0.83	1.18
PC7	0.40	147	312	55	1,331	0	0	0	0	570	0	0	0.83	0.94
PC8	0.40	147	312	55	1,198	0	0	0	0	703	0	0	0.83	0.94
PC9	0.40	147	312	55	1,197	0	0	0	0	703	0	0	0.83	1.09
GC1*	0.45	151	335	0	0	0	0	872	0	0	1,060	0	0.02	0.63
GC2*	0.45	151	335	0	872	0	0	0	0	0	1,060	0	0.02	0.63
GC3*	0.45	151	335	0	872	0	0	0	0	0	1,060	0	0.02	0.63
GC4*	0.45	151	335	0	654	0	0	218	0	0	1,060	0	0.02	0.63
GC5*	0.45	151	335	0	654	0	0	218	0	0	1,060	0	0.02	0.63
GC6*	0.45	151	335	0	436	0	0	436	0	0	1,060	0	0.02	0.63
GC7*	0.45	151	335	0	436	0	0	436	0	0	1,060	0	0.02	0.63
GC8*	0.45	151	335	0	218	0	0	654	0	0	1,060	0	0.02	0.63
GC9*	0.45	151	335	0	218	0	0	654	0	0	1,060	0	0.02	0.63
GC10 _§	0.42	142	338	0	0	1,178	0	0	0	0	709	0	0.00	0.00
GC11 _§	0.42	142	338	0	0	0	0	0	1279	0	709	0	0.00	0.00
GC12 _§	0.42	142	338	0	1,205	0	0	0	0	0	714	0	0.00	0.00
GC13 _§	0.42	142	338	0	1,205	0	0	0	0	0	0	690	0.00	0.00
GC14 _§	0.42	142	338	0	1,219	0	0	0	0	0	0	698	0.00	0.00

Aggregates: LS (Limestone), GV (Natural gravel), SS (Sandstone), GR (Granite), DM (Dolomite), UKN (Unknown), NS (Siliceous natural sand).

*Five different surface treatments were applied for each mixture (see **Table 2**).

§Four different surface treatments were applied for each mixture (see **Table 2**).

The detailed information of DFT and CTM collected from the literature is summarized in **Figure 14** through **Figure 19**. The result of DFT60 (DFT at 60 km/h) obtained from Dataset 2 was converted into DFT20 for the calculation of IFI friction. This is because the results of DFT20 and CTM are needed to calculate IFI friction at 60 km/h (F60) and slip speed (S_p), which are beneficial for the normalization of friction measurements with different equipment to a common calibrated index in accordance with ASTM E1960-07. For this purpose, equivalent DFT20 in Dataset 2 was estimated using the linear relationship in **Figure 20** ($DFT20 = 0.9414 \times DFT60$), which was calculated by referring to the results from [29].

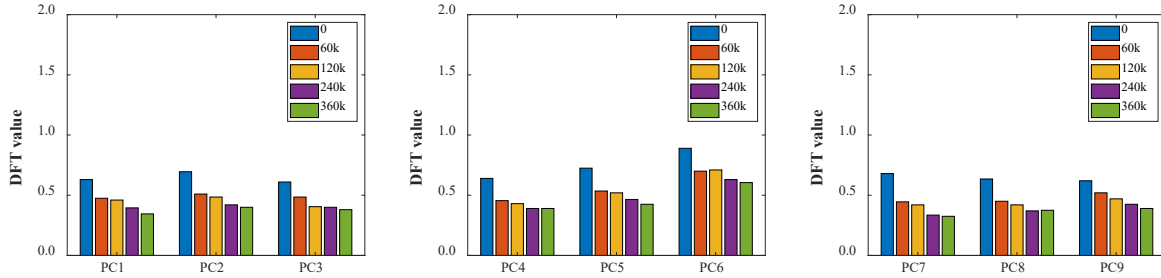


Figure 14. DFT20 of plain concrete at 0–360k polishing (Dataset 1: PC1–9).

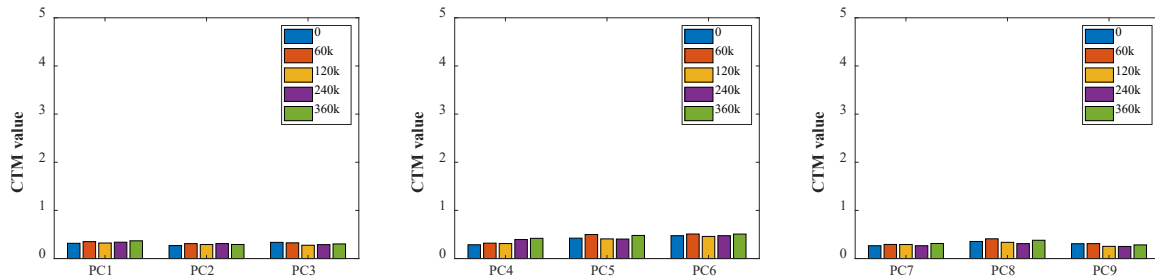


Figure 15. CTM of plain concrete at 0–360k polishing (Dataset 1: PC1–9).

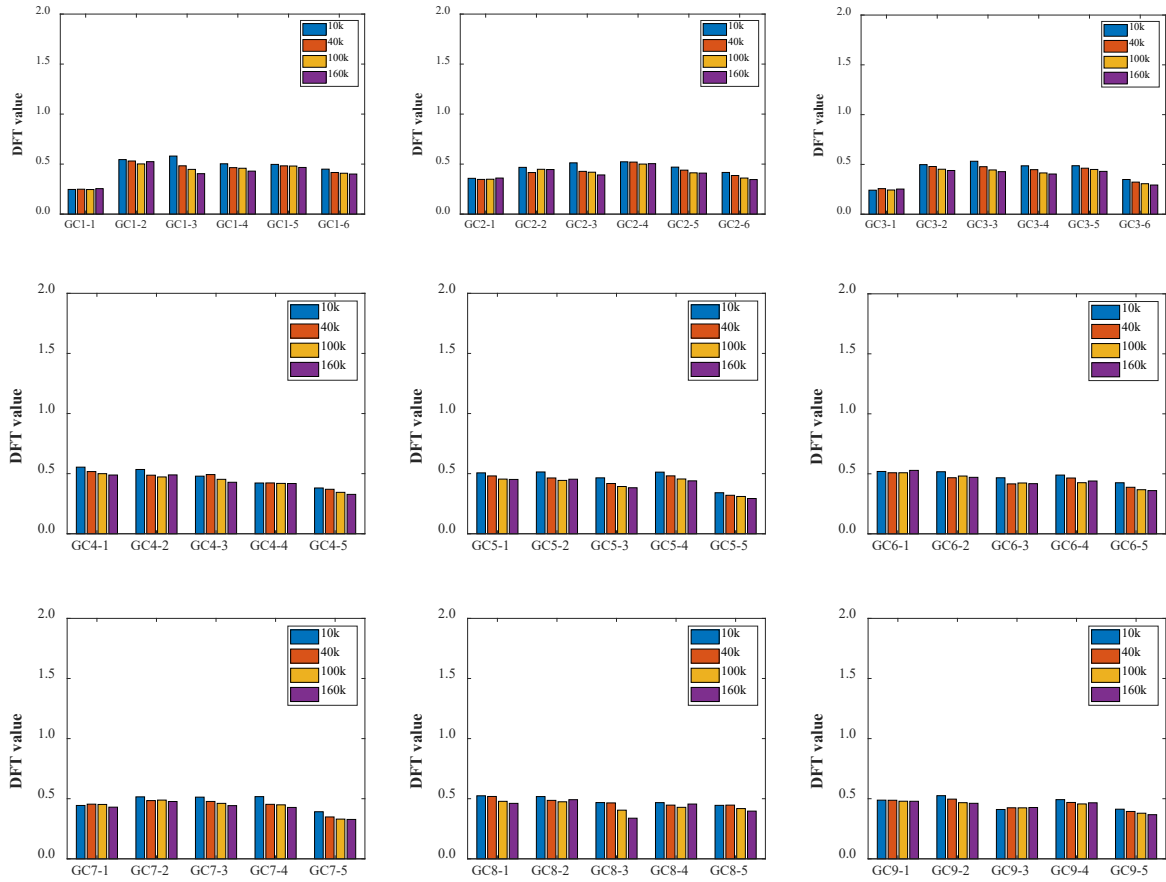


Figure 16. DFT20 of ground/grooved concrete at 10k–160 k polishing (Dataset 2: GC1–9).

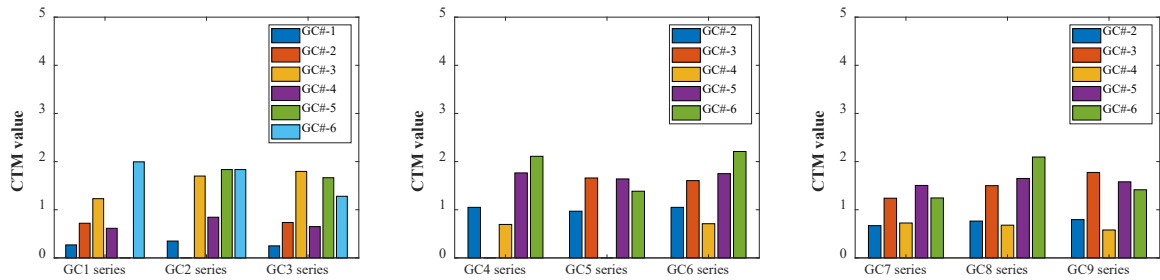


Figure 17. CTM of ground/grooved concrete at 160k polishing (Dataset 2: GC1–9).

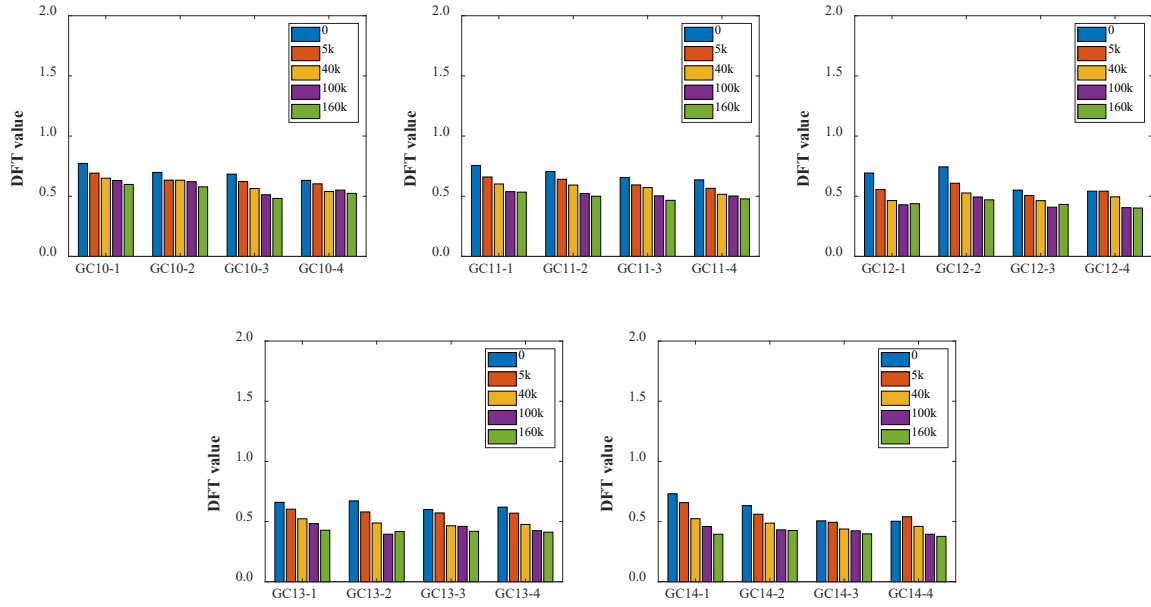


Figure 18. DFT20 of ground/grooved concrete at 0k–160 k polishing (Dataset 3: GC10–14).

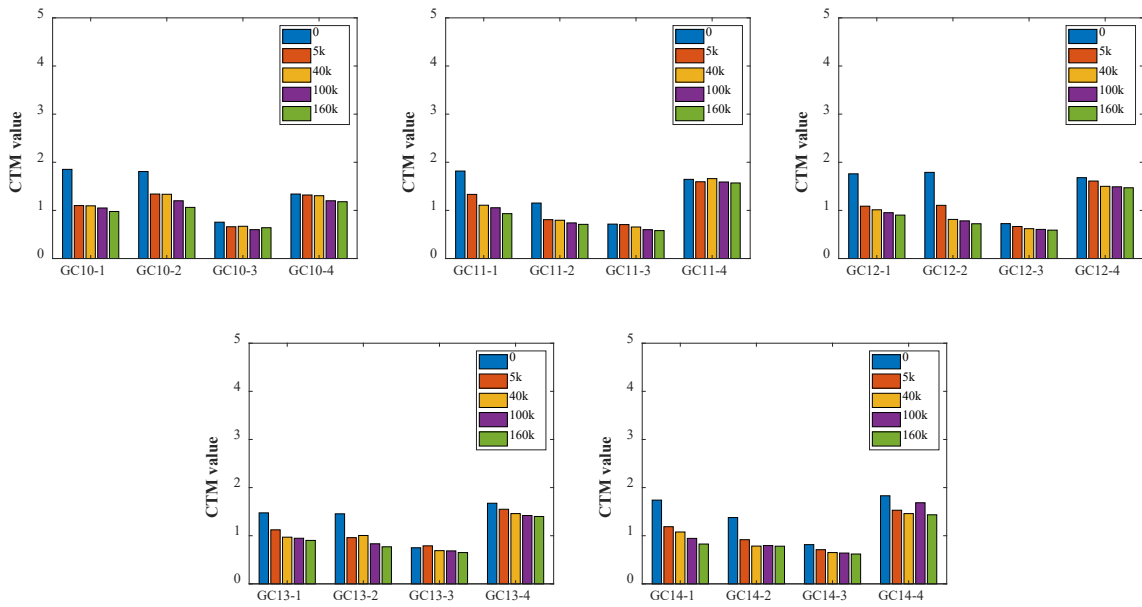


Figure 19. CTM of ground/grooved concrete at 0–160k polishing (Dataset 3: GC10–14).

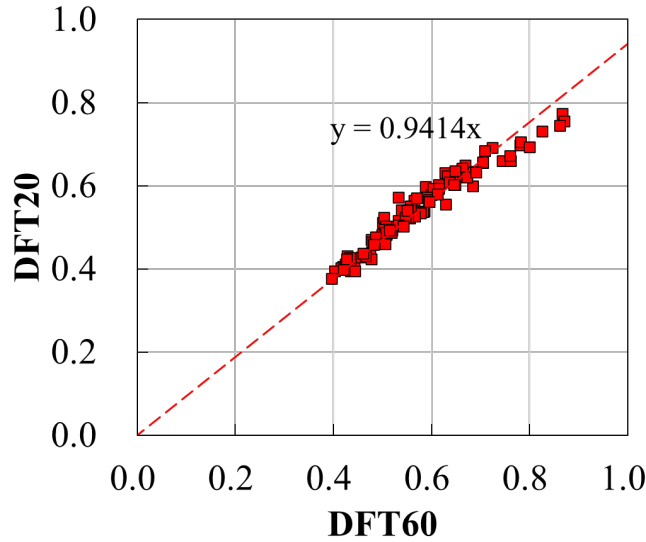


Figure 20. Linear relationship between DFT60 and DFT20.

Based on the developed database, 21 inputs and 2 outputs were selected for the ANN model. These are listed in **Table 4**. Mixture proportions of concrete, characteristics of concrete surface, and number of accelerated polishing cycles were used as input parameters due to their significant effects on the frictional properties of pavement. Friction (DFT20) and texture (CTM) at a given number of polishing cycles were designated as outputs. Because of different number of data points for DFT20 (553) and CTM (265), two separate ANN models were developed, one for each output.

Table 4. Inputs and outputs used for the ANN model.

Parameters	
Inputs	<p>Mixture proportion parameters (14): w/cm; water content (kg/m³); portland cement content (kg/m³); fly ash content (kg/m³); coarse aggregates type (LS, GV, SS, GR, and DM); fine aggregates type (LS, NS, and UKN); air-entraining agent; water-reducing agent.</p> <p>Grinding and grooving parameters (6): Spacer, blade thickness, and depth of grinding; Same information for grooving.</p> <p>Number of polishing cycles (1)</p>
Outputs	DFT20; CTM

CHAPTER 3

Findings

DETERMINATION OF ANN STRUCTURE

To prevent overfitting and underfitting and improve accuracy, the structure of ANN should be carefully selected in terms of the numbers of hidden layers and hidden neurons. There is no general method to determine suitable numbers of hidden layers and neurons. Most practical problems do not involve a large number of hidden layers, so use of the ANN model is not needed, thus avoiding a significant increase in computational cost. With respect to hidden neurons, the number of neurons usually less than the number of input variables. Therefore, in the preliminary tests to determine the ANN structure, the ANN models having 1–3 hidden layers and 1–10 neurons were tested. The input and output parameters used for the preliminary tests are provided in **Table 4**. To improve the reliability of the results, the inner 5-fold cross validation was applied. Details of the computing resources used for the analysis are as follows: Intel(R) Core i5-9400 CPU (2.9 GHz) and 16 GB RAM.

The prediction errors of the ANN model having different numbers of hidden layers and neurons are provided in **Table 5** and **Table 6**. The ANN model with 1 hidden layer and 4 hidden neurons shows the lowest MAE for DFT20 (7.6%) and CTM (12.2%). This model also had a low level of RMSE for DFT20 (0.044) and CTM (0.15). Thus, the ANN model having 1 hidden layer and 4 hidden neurons was selected for further analysis. It should be noted that, based on the preliminary analysis of the results, the choice of polishing device had a small impact on the prediction accuracy of the ANN model, whereas that of the number of polishing cycles was more dominant.

Table 5. Evaluation of prediction error for DFT20 depending on the numbers of hidden layers and hidden neurons.

MAE Hidden neurons	1	2	3	4	5	6	7	8	9	10
Hidden layers 1	9.1%	8.1%	8.2%	7.6%	7.8%	7.9%	7.8%	7.7%	7.9%	8.0%
Hidden layers 2	10.2%	8.1%	7.8%	8.0%	7.8%	8.0%	7.8%	7.8%	8.2%	7.8%
Hidden layers 3	8.8%	8.3%	8.1%	7.9%	8.5%	7.8%	8.1%	8.3%	7.9%	7.9%
RMSE Hidden neurons	1	2	3	4	5	6	7	8	9	10
Hidden layers 1	0.052	0.048	0.048	0.044	0.046	0.045	0.045	0.046	0.046	0.045
Hidden layers 2	0.058	0.048	0.046	0.046	0.045	0.046	0.045	0.047	0.047	0.046
Hidden layers 3	0.051	0.049	0.048	0.047	0.049	0.045	0.047	0.048	0.045	0.045

Table 6. Evaluation of prediction error for CTM depending on the numbers of hidden layers and hidden neurons.

MAE Hidden neurons	1	2	3	4	5	6	7	8	9	10
Hidden layers 1	18.7%	15.7%	12.5%	12.2%	13.1%	13.5%	12.9%	13.5%	13.0%	14.2%
Hidden layers 2	16.4%	14.6%	13.6%	13.1%	12.3%	13.1%	12.8%	12.9%	12.5%	14.3%
Hidden layers 3	16.4%	15.3%	15.0%	13.2%	13.2%	12.3%	12.4%	13.8%	12.5%	14.5%
RMSE Hidden neurons	1	2	3	4	5	6	7	8	9	10
Hidden layers 1	0.19	0.17	0.15	0.15	0.16	0.16	0.16	0.16	0.16	0.15
Hidden layers 2	0.18	0.16	0.16	0.15	0.16	0.16	0.16	0.16	0.16	0.16
Hidden layers 3	0.17	0.17	0.16	0.16	0.16	0.16	0.15	0.16	0.16	0.16

ANN-BASED PREDICTION RESULTS

Prediction of Friction and Texture using the ANN Model

Using the ANN architecture selected from the previous section, the ANN-based prediction showed high prediction accuracies for DFT20 and CTM. As shown in **Figure 21**, the correlation coefficients (R) for DFT20 and CTM are 0.90893 and 0.96335, respectively. The MAEs for DFT20 and CTM are 6.0% and 11.7%, respectively (see **Table 7**). The RMSEs of DFT20 and CTM are 0.42 and 0.99. The high prediction accuracy for DFT20 indicated that the relationship of concrete constituents, polishing, and characteristics of surface treatment with DFT20 is better than that with CTM. This might be attributable to different polishing resistances of cementitious matrix and aggregates, which can be also observed in asphalt concrete pavement [61].

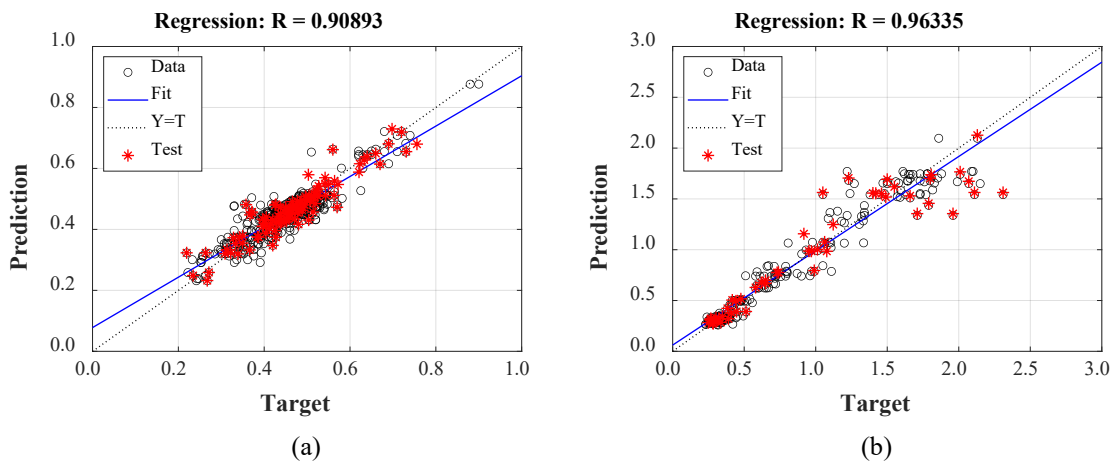


Figure 21. Prediction results using ANN: (a) DFT20 and (b) CTM.

Table 7. MAE and RMSE of DFT20 and CTM.

Tests	MAE	MAE	RMSE	RMSE
	Avg. validation	Test	Avg. validation	Test
DFT20	7.6%	6.0%	0.044	0.039
CTM	12.2%	11.7%	0.15	0.22

Sensitivity Analysis

The relative importance of input variables was studied through a sensitivity analysis for the ANN model. As a sensitivity analysis, weight analysis can be employed to explain the relationship between input variables and output variables in the ANN model. The weight analysis computes the strength of the connections between the input factors and the output factors quantitatively [62,63]. The percentages of the influence of input variable on the output value, Q_{ik} , can be expressed as

$$Q_{ik}(\%) = \frac{\sum_{j=1}^N ((|w_{ij}| / \sum_{i=1}^M |w_{ij}|) \cdot |v_{jk}|)}{\sum_{i=1}^M (\sum_{j=1}^N ((|w_{ij}| / \sum_{i=1}^M |w_{ij}|) \cdot |v_{jk}|))} \times 100\%$$

where w_{ij} represents the weights between the input neuron i and the hidden neuron j , and v_{jk} represents the weights between the hidden neuron j and the output neuron k . The ANN structure used in this study had

1 hidden layer and 4 neurons. The numbers of inputs and outputs are 21 and 1, respectively. The contributions of each input on the output of DFT20 and CTM are provided in **Figure 22**. The influences of inputs on DFT20 and CTM were similar. Meanwhile, it was found that polishing cycles highly influenced the prediction of CTM.

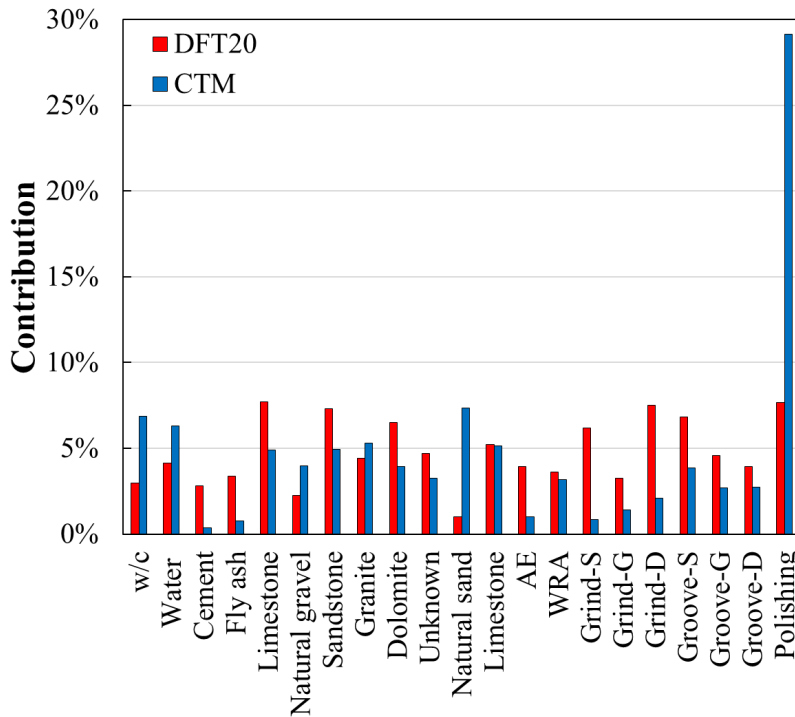


Figure 22. Contribution of input parameters on DFT20 and CTM (Grind- or Groove- S, G, and D means spacer, gap, and depth, respectively).

IFI Friction and Skid Number

Using predicted DFT and CTM values, the IFI of friction parameters at 60 km/h (F_{60}) and slip speed (S_p) were calculated. To compare and normalize texture and friction measured by different devices, PIARC performed international experiments in 1992 from 16 countries [23,54]. The tests using a total of 51 different measurement systems were conducted at 54 sites. Various types of friction testing equipment, such as locked-wheel, fixed slip, side force, and British pendulum test, were used. Surface texture of pavement was measured by the volumetric sand patch, laser profilometers, optical system, and outflow meters.

These IFI friction parameters of S_p and F_{60} can be computed in accordance with ASTM E1960-07. The slip speed in a unit of km/h is determined from the mean profile depth (MPD) obtained from CTM in a unit of mm as follows:

$$S_p = 14.2 + 89.7MPD$$

Friction (FR) measured by a device on wet pavement at a given speed (S) and S_p can be used for calculating FR at 60 km/h using the following relationship:

$$FR_{60} = FR(S) \cdot e^{\frac{S-60}{S_p}}$$

where $FR60$ represents adjusted value of FR at 60 km/h and $FR(S)$ represents friction value at speed of S . The linear relationship between IFI $F60$ and $FR60$ can be expressed as:

$$F60 = A + B \cdot FR60$$

where A and B are calibrated constants. Combining the Eqs. 10 and 11, $F60$ can be expressed with respect to the FR and S_p :

$$F60 = A + B \cdot FR(S) \cdot e^{\frac{S-60}{S_p}}$$

The coefficients of A and B are 0.0082 and 0.732 for the DFT20 as provided in ASTM E1960-07. Then, IFI $F60$ can be calculated as follows:

$$F60 = 0.081 + 0.732 \cdot DFT20 \cdot e^{\frac{40}{S_p}}$$

IFI $F60$ and S_p are also used for calculating equivalent friction obtained from different devices. In this study, predicted results were normalized based on the locked-wheel skid trailer method [64], which is known as the widely used method for measuring pavement friction in the United States in accordance with ASTM E 274/274M-15. The equivalent skid number ($FR65$) measured by a locked-wheel skid trailer at 65 km/h (~40 mph) using a smooth tire in accordance with ASTM E524-08 can be computed using the following formula:

$$FR65_S = \frac{F60 - A_{IFI}}{B_{IFI}} \frac{1}{e^{\frac{5}{S_p}}}$$

where $FR65_S$ indicates results of $FR65$ using a smooth tire and coefficients of A_{IFI} and B_{IFI} are equal to 0.045 and 0.925, respectively [6,29,54]. Note that skid number at 65 km/h ($SN65_S$) is equal to the friction $FR65_S$ multiplied by 100.

A high prediction accuracy for $SN65_S$ was observed as shown in **Figure 23**. Using the selected weight and bias, the prediction of $SN65_S$ for all concrete mixtures was conducted. Target and predicted $SN65_S$ were calculated using target and predicted IFI parameters. Note that predicted IFI parameters were calculated using predicted DFT20 and CTM. The average MAE for $SN65_S$ was 7.2%, which means that the ANN model provides accurate predictions for frictional properties based on the information of concrete constituents, surface treatment, and polishing cycles. In the Data 2, target $SN65_S$ of GC1-5, GC2-2, GC4-3, and GC5-4 were not provided due to the lack of their CTM values. Even though their exact values (target) were unknown, their CTM as well as $SN65_S$ can be estimated using the ANN model. Predicted $SN65_S$ for GC1-5, GC2-2, GC4-3, and GC5-4 are 30.6, 27.4, 31.6, and 24.4, respectively.

Prediction of Long-term Skid Number

Based on the prediction results provided in the previous section, the long-term frictional properties of plain and ground and grooved concrete, up to 500K polishing cycles, were estimated. This extrapolation process can reduce the cost, time, and resources for the additional experimental work. In this section, comparative analysis of the ANN-based prediction and experimental results-based regression was performed to prove the high performance of the ANN model. The ANN-based prediction was conducted by increasing the number of polishing cycles. For the results-based regression, which has also been used for estimating the friction of pavement [65], power law equation was adopted: $y = (x/a)^{1/b}$. The coefficients used for this

equation are provided in **Table 8**. It should be noted that PC and GC means plain and ground and grooved concrete, respectively. The results of SN_{65s} using two different methods are provided in **Figure 24** and **Figure 25**. The ANN-based prediction results showed a better agreement than the regression curve, which might be attributed by the consideration of various kinds of inputs, which can influence the frictional properties. It should be noted that the results from Data 2 were not analyzed due to the lack of CTM at different polishing cycles (only CTM at 160k is provided from the literature).

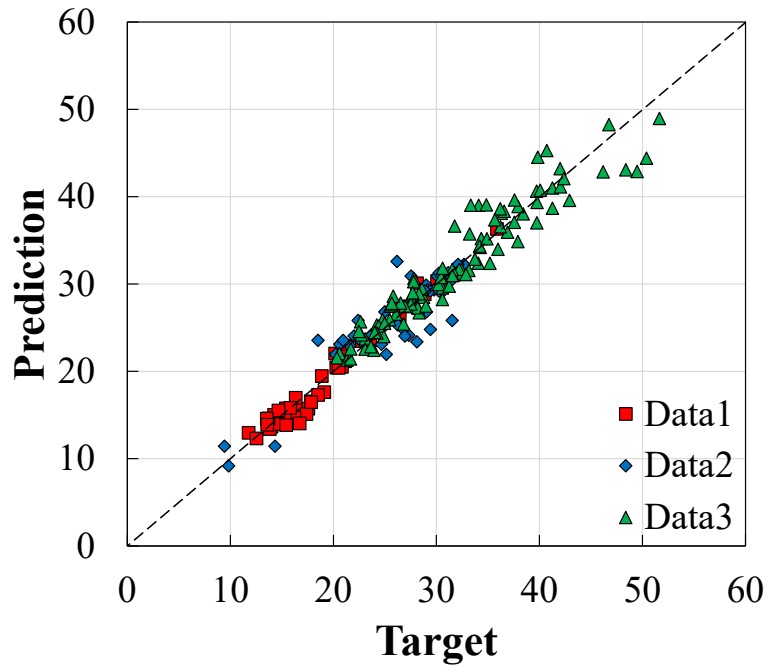


Figure 23. Prediction results for the skid number at 65 km/h (SN_{65s}).

Table 8. Coefficients for power-law regression model.

Samples	Coefficient a	Coefficient b	Samples	Coefficient a	Coefficient b
PC1	$3.817 \cdot 10^8$	-0.489	GC11-3	$1.026 \cdot 10^8$	-0.286
PC2	$3.476 \cdot 10^8$	-0.487	GC11-4	$2.792 \cdot 10^{11}$	-0.445
PC3	$4.595 \cdot 10^7$	-0.380	GC12-1	$5.104 \cdot 10^{10}$	-0.506
PC4	$3.652 \cdot 10^6$	-0.187	GC12-2	$3.684 \cdot 10^8$	-0.310
PC5	$4.432 \cdot 10^8$	-0.386	GC12-3	$2.399 \cdot 10^8$	-0.364
PC6	$1.662 \cdot 10^{10}$	-0.413	GC12-4	$4.307 \cdot 10^8$	-0.295
PC7	$1.289 \cdot 10^7$	-0.317	GC13-1	$3.701 \cdot 10^7$	-0.217
PC8	$6.589 \cdot 10^6$	-0.227	GC13-2	$1.177 \cdot 10^7$	-0.198
PC9	$1.552 \cdot 10^9$	-0.633	GC13-3	$3.557 \cdot 10^8$	-0.355
GC10-1	$5.436 \cdot 10^9$	-0.303	GC13-4	$6.883 \cdot 10^9$	-0.390
GC10-2	$1.045 \cdot 10^9$	-0.256	GC14-1	$4.372 \cdot 10^6$	-0.145
GC10-3	$4.332 \cdot 10^9$	-0.425	GC14-2	$5.082 \cdot 10^{10}$	-0.540
GC10-4	$2.155 \cdot 10^{12}$	-0.506	GC14-3	$6.377 \cdot 10^9$	-0.520
GC11-1	$8.070 \cdot 10^8$	-0.279	GC14-3	$2.531 \cdot 10^8$	-0.286
GC11-2	$3.741 \cdot 10^8$	-0.298			

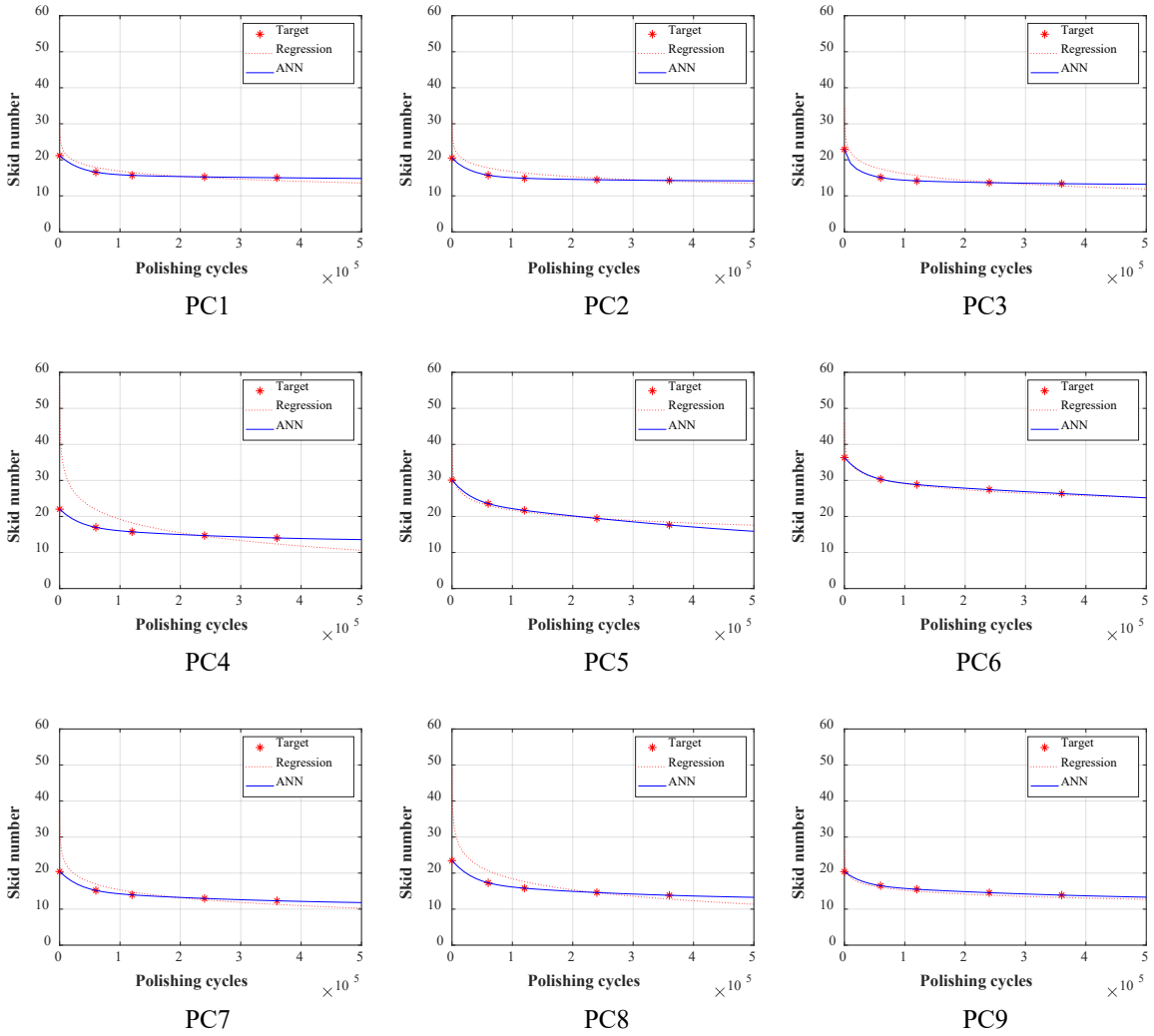
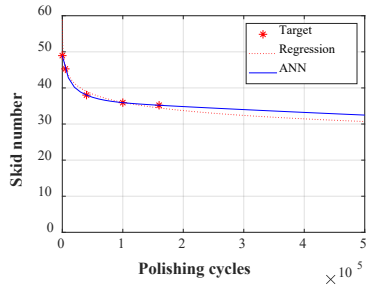
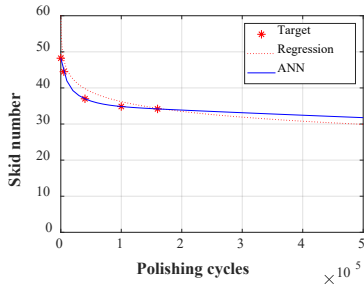


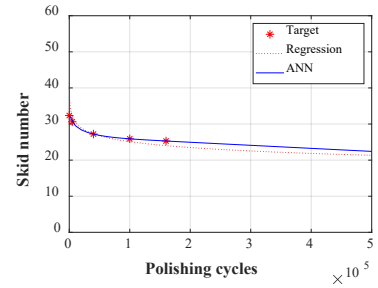
Figure 24. Predicted long-term frictional properties of plain concrete pavement.



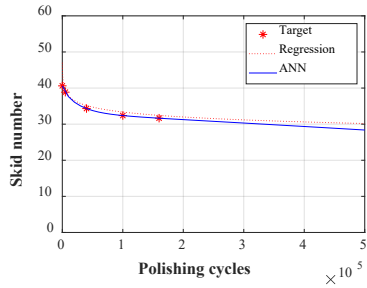
GC10-1



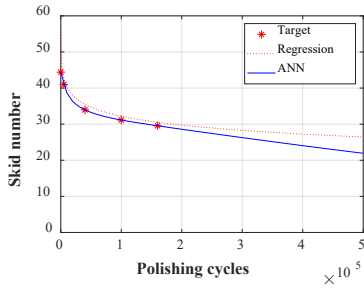
GC10-2



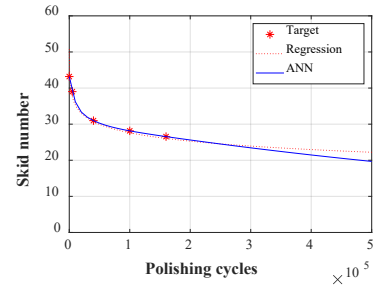
GC10-3



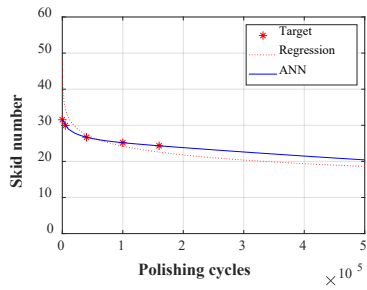
GC10-4



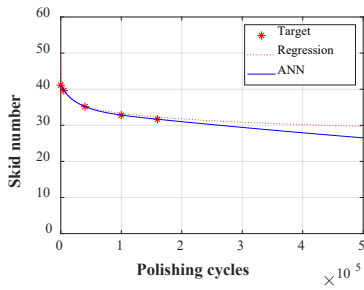
GC11-1



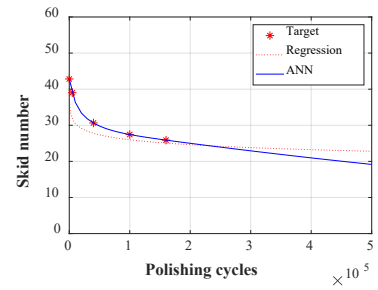
GC11-2



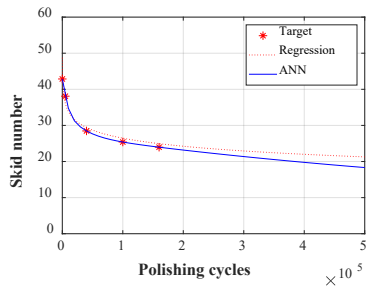
GC11-3



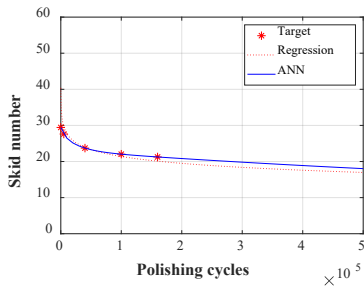
GC11-4



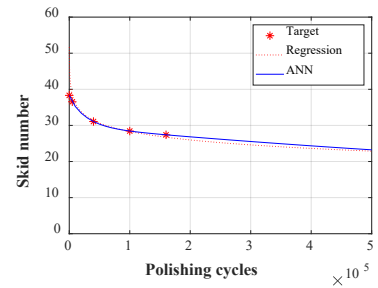
GC12-1



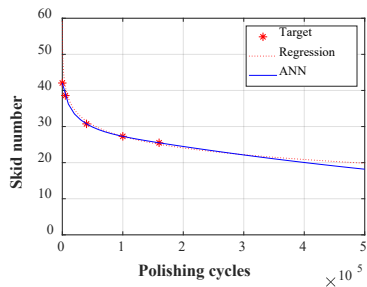
GC12-2



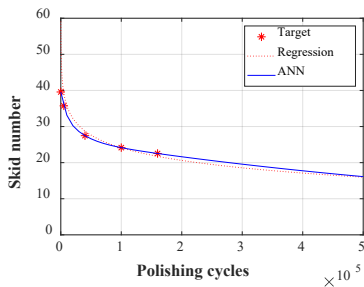
GC12-3



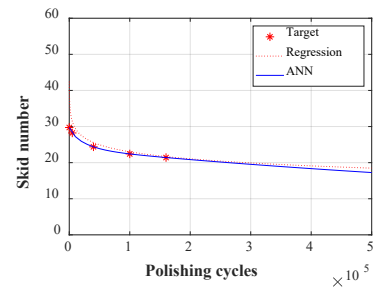
GC12-4



GC13-1



GC13-2



GC13-3

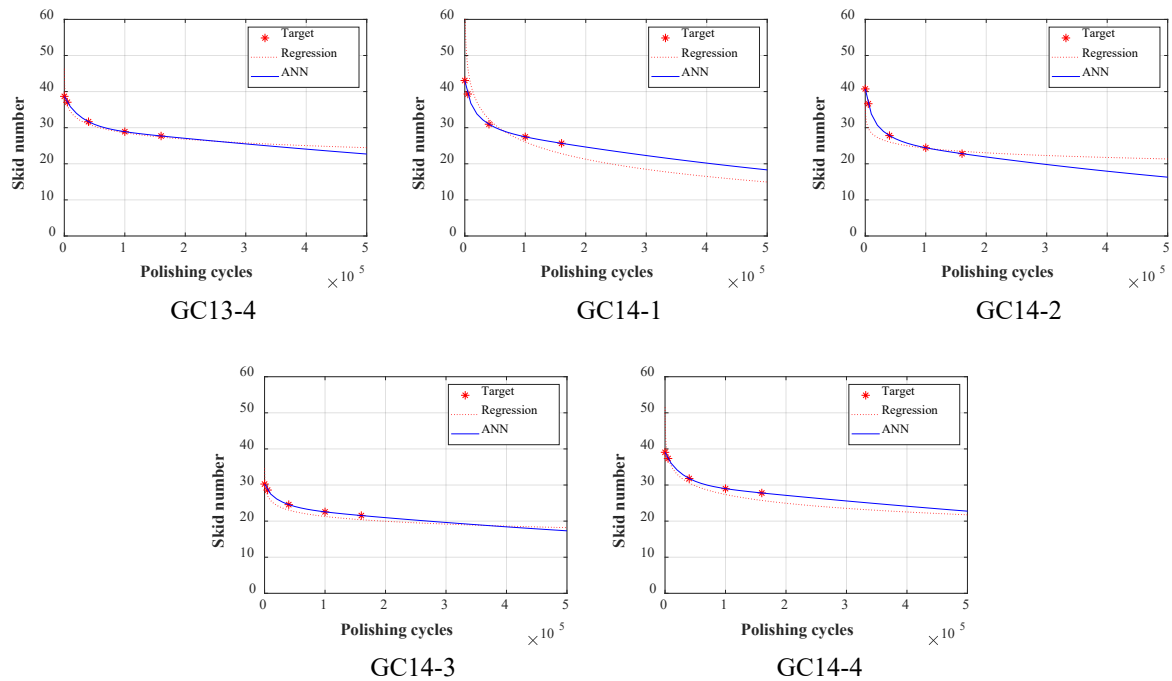


Figure 25. Predicted long-term frictional properties of ground/grooved concrete pavement.

Estimation of Terminal Friction

With the use of ANN-based predictions of long-term frictional properties of concrete pavement, the terminal friction value can be estimated. Change of friction of concrete pavement as a function of polishing can be plotted, as can be seen in **Figure 26**. It should be noted that friction degradation of concrete pavement can be varied depending on the characteristics of the concrete pavement (e.g., concrete constituents, grinding, etc.). The adequate friction level is maintained or sometimes increased after construction (Stage1). A slight increase of friction number was observed in diamond-ground concrete pavement (US-50) provided in [57]. Meanwhile, Stage 1 is not observed in some concrete pavements (e.g., diamond-ground concrete pavement (US-24) [57], various types of surface textured concrete pavements [66], and experimental results from [6,29,50]). These concrete pavements showed friction loss as the degree of polishing increased (Stage 2). After a significant friction loss caused by polishing, the friction value is maintained, as can be seen in the friction stabilization zone (Stage 3). In this stage, the friction is very slowly decreased regardless of additional polishing or weathering condition. As specified, the rate of friction loss and terminal friction are highly related to the polishing resistance properties of cementitious matrix and aggregates. Therefore, the ANN-based model, which can characterize the relationship of concrete constituents and polishing with frictional properties, is suitable for estimating terminal friction of plain and ground and grooved concrete.

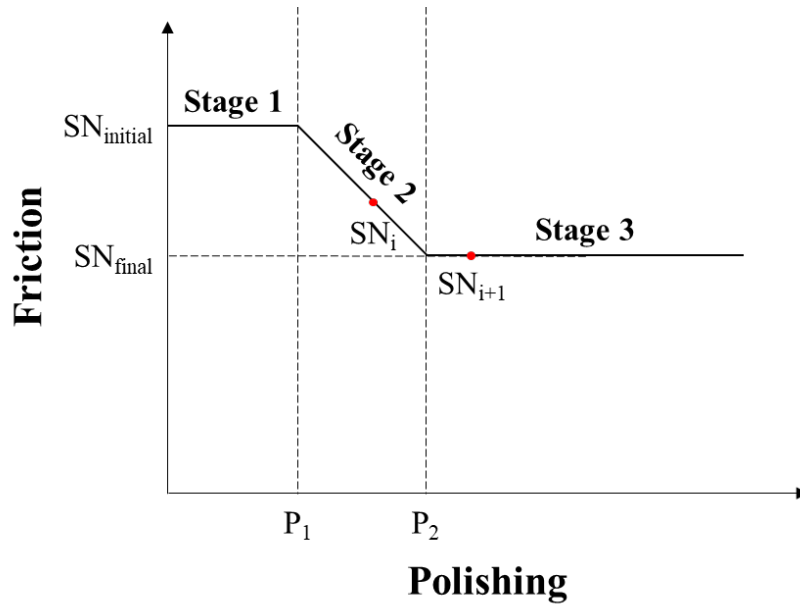


Figure 26. Lifecycle of pavement depending on degree of polishing [65].

To determine terminal friction of concrete pavement, the analysis of normalized standard deviation (STD) of SN_{65S} was performed. The STD value of 5 neighboring SN_{65S} as a function of polishing cycles was first calculated using the following equation:

$$STD = \sqrt{\frac{1}{N-1} \sum_{i=1}^N |A_i - \bar{A}_i|^2}$$

where N is equal to number of testing neighbors, A_i represent SN_{65S} , and \bar{A}_i represents the mean of A_i . For example, the STD of SN_{65S} at 100k can be obtained from SN_{65S} in a range of 80k–120k. Here, the interval of polishing is equal to 10k. Subsequently, the normalization for STD was employed to minimize the effect of high or low level of SN_{65S} . To determine the plateau value (terminal friction), the appropriate threshold of the normalized STD should be selected. In this study, the normalized STD of 0.05 was selected as a threshold due to a small decrease in the ratio of neighboring normalized STD, less than 5%. As can be seen in **Figure 27** (sample of GC14-4), the variation of normalized STD in the red area (Stage 3 - friction stabilization zone) is very small.

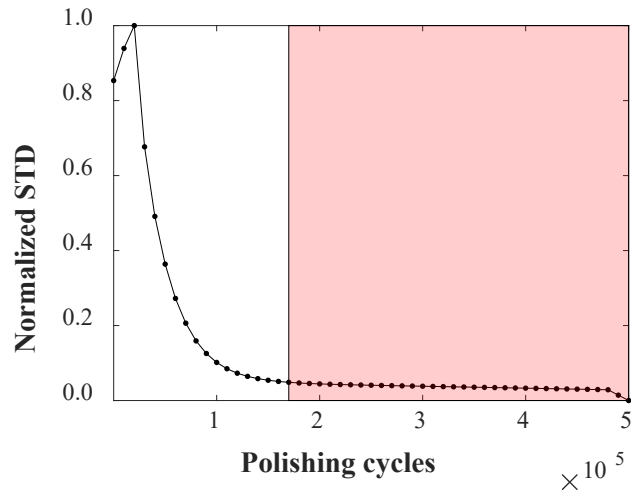


Figure 27. Determination of polishing cycles in a plateau of normalized STD of GC14-4's SN65s to identify terminal SN65s.

Using the ANN model, the terminal friction value and polishing cycles are identified as provided in **Table 9**. In a comparison to the skid numbers at the final polishing cycles from the Data 1–3, the difference is as small as 4.7%. It is expected that this reliable and robust method can also be applicable for evaluating terminal friction of pavements.

Concrete pavement having a high terminal friction is recommended to prevent traffic accidents. It was reported that the skid number of pavements measured by locked-wheel test with a smooth tire should be higher than 20 or 23 for preventing car accidents caused by low-level skid resistance [67]. The applicable concrete mixtures that satisfy this recommendation are as follows. In the case of plain concrete, PC6 had terminal friction of 27.7. This mixture had a relatively higher ratio of fine aggregate (70% UKN) to coarse aggregate (30% LS). Most of the ground and grooved concrete samples showed a high terminal skid number, which satisfied the recommendation. Even though GC13-3 and GC14-3 showed relatively low skid numbers compared to other samples, their terminal frictions were very close to the recommendation. The relatively low friction of GC13 and GC14 series might be attributable to the use of coarse and fine limestone aggregates, which have poor polishing resistance properties. Similarly, plain concrete incorporating coarse limestone aggregates generally showed low terminal friction. Furthermore, the third grinding method of Data 3 (spacer = 0.076 cm, blade thickness = 0.06 cm, depth = 0.159 cm) should be avoided due to its relatively poor enhancement of initial and terminal frictions. Based on these analyses, grooved concrete pavement that incorporates natural gravel and natural sand is recommended for long-term polishing-resistant concrete pavement.

Table 9. The ANN-based estimation of terminal friction of plain and ground and grooved concrete.

Samples	Measurement	Measurement	ANN	ANN	Samples	Measurement	Measurement	ANN	ANN
	Initial SN65 _s *	Final SN65 _s **	Terminal SN65 _s	Polishing cycles		Initial SN65 _s *	Final SN65 _s **	Terminal SN65 _s	Polishing cycles
PC1	21.1	14.2	15.6	140k	GC11-3	33.1	22.5	23.4	230k
PC2	20.8	14.1	14.8	140k	GC11-4	42.0	32.2	29.7	280k
PC3	21.3	13.8	14.2	110k	GC12-1	46.2	25.5	26.6	130k
PC4	20.1	16.7	14.6	260k	GC12-2	49.5	24.9	24.9	120k
PC5	28.1	19.1	16.4	450k	GC12-3	28.6	21.3	21.5	140k
PC6	35.9	26.4	27.7	220k	GC12-4	36.6	27.3	27.5	150k
PC7	20.3	12.5	13.0	230k	GC13-1	42.4	25.0	24.5	200k
PC8	22.7	15.4	14.6	240k	GC13-2	42.9	23.1	22.8	150k
PC9	20.5	13.6	14.2	300k	GC13-3	31.2	21.6	20.0	260k
GC10-1	51.6	34.3	35.9	100k	GC13-4	41.3	27.5	27.4	180k
GC10-2	46.7	34.2	34.8	100k	GC14-1	48.4	22.6	25.2	180k
GC10-3	35.2	24.2	25.8	110k	GC14-2	40.1	23.6	23.3	140k
GC10-4	39.7	32.4	32.1	120k	GC14-3	27.8	20.3	20.4	240k
GC11-1	50.4	30.6	30.0	140k	GC14-4	34.8	25.6	27.6	170k
GC11-2	42.0	26.1	27.3	130k					

*: SN65_s at 0k for plain concrete and at 10k for ground and grooved concrete provided in [6].

** : SN65_s at 360k for plain concrete and at 160k for ground and grooved concrete provided in [29].

CHAPTER 4

Conclusions

The adequate long-term frictional properties of concrete pavement are crucial for ensuring the safety of drivers. Experimental studies have identified several factors influencing pavement friction, including concrete mixture proportion, types of aggregates, degree of pavement polishing, and surface texturing techniques. However, conventional linear and non-linear regression models are not appropriate to analyze the complex relationship between these factors and concrete pavement friction. Therefore, this study adopted the use of the ANN model to predict and estimate long-term frictional properties of plain and ground/grooved concrete pavement. The following conclusions can be drawn for the ANN-based model for concrete pavement.

- To train the ANN-based model, data of plain and ground/grooved concrete mixture proportion, degree of polishing, types of aggregates, characteristics of grinding and grooving, friction (DFT), and texture (CTM) were collected. Using 553 DFT and 265 CTM data, the ANN model was developed, which showed good prediction results.
- The ANN model used for the prediction of DFT and CTM has 1 hidden layer and 4 hidden neurons, which was determined based on a preliminary test. This ANN model showed 6.0% and 11.7% error for DFT and CTM, respectively.
- Using the ANN model, the long-term frictional properties of concrete pavement beyond the accelerated testing ranges provided in the literature were estimated. In a comparison to a regression model, the ANN model showed better agreement.
- The terminal friction of concrete pavement was evaluated based on predicted long-term friction. With the use of a normalized STD method proposed by this research, the terminal friction of concrete pavement can be calculated. Based on this result, concrete pavement having a high long-term friction can be identified.

References

- [1] Hall, J.W., K.L. Smith, L. Titus-Glover, J.C. Wambold, T.J. Yager, and Z. Rado (2009). *Guide for Pavement Friction*, National Cooperative Highway Research Program Web-Only Document 108, Washington, DC: The National Academies Press. <https://doi.org/10.17226/23038>.
- [2] Yoshitake, I., S. Ueno, Y. Ushio, H. Arano, and S. Fukumoto (2016). Abrasion and skid resistance of recyclable fly ash concrete pavement made with limestone aggregate, *Constr. Build. Mater.* 112:440–446. <https://doi.org/10.1016/j.conbuildmat.2016.02.185>.
- [3] Rith, M., Y.K. Kim, and S.W. Lee (2020). Characterization of long-term skid resistance in exposed aggregate concrete pavement, *Constr. Build. Mater.* 256:119423. <https://doi.org/10.1016/j.conbuildmat.2020.119423>.
- [4] Wang, H., and R.Y. Liang (2014). Predicting Field Performance of Skid Resistance of Asphalt Concrete Pavement, In: *American Society of Civil Engineers (ASCE)*, 2014:296–305. <https://doi.org/10.1061/9780784413418.030>.
- [5] Hofko, B., H. Kugler, G. Chankov, and R. Spielhofer (2019). A laboratory procedure for predicting skid and polishing resistance of road surfaces, *Int. J. Pavement Eng.* 20:439–447. <https://doi.org/10.1080/10298436.2017.1309191>.
- [6] Rado, Z. (2009). *Evaluating Performance of Limestone Prone to Polishing*, Report No. FHWA-PA-2009-022-510401-015, University Park, PA: Larson Transportation Institute.
- [7] Cho, C. (2010). *Application of Hilbert Huang Transformation to Analyze Pavement Texture-Friction Relationship*, Masters Thesis, The Pennsylvania State University.
- [8] Kim, H., E. Ahn, S. Cho, M. Shin, and S.H. Sim (2017). Comparative analysis of image binarization methods for crack identification in concrete structures, *Cem. Concr. Res.* 99:53–61. <https://doi.org/10.1016/j.cemconres.2017.04.018>.
- [9] Jeyasehar, C.A., and K. Sumangala (2006). Damage assessment of prestressed concrete beams using artificial neural network (ANN) approach, *Comput. Struct.* 84:1709–1718. <https://doi.org/10.1016/j.compstruc.2006.03.005>.
- [10] Kim, B., and S. Cho (2019). Image-based concrete crack assessment using mask and region-based convolutional neural network, *Struct. Control Heal. Monit.* 26:e2381. <https://doi.org/10.1002/stc.2381>.
- [11] Yoon, J.Y., H. Kim, Y.-J. Lee, and S.-H. Sim (2019). Prediction Model for Mechanical Properties of Lightweight Aggregate Concrete Using Artificial Neural Network, *Materials (Basel)*. 12:2678.
- [12] Uysal, M., and H. Tanyildizi (2012). Estimation of compressive strength of self compacting concrete containing polypropylene fiber and mineral additives exposed to high temperature using artificial neural network, *Constr. Build. Mater.* 27:404–414. <https://doi.org/10.1016/j.conbuildmat.2011.07.028>.
- [13] Vakharia, V., and R. Gujar (2019). Prediction of compressive strength and portland cement composition using cross-validation and feature ranking techniques, *Constr. Build. Mater.* 225:292–301. <https://doi.org/10.1016/j.conbuildmat.2019.07.224>.

- [14] Yadollahi, A., E. Nazemi, A. Zolfaghari, and A.M. Ajorloo (2016). Optimization of thermal neutron shield concrete mixture using artificial neural network, *Nucl. Eng. Des.* 305:146–155. <https://doi.org/10.1016/j.nucengdes.2016.05.012>.
- [15] Zhang, J., Y. Huang, G. Ma, and B. Nener (2021). Mixture optimization for environmental, economical and mechanical objectives in silica fume concrete: A novel framework based on machine learning and a new meta-heuristic algorithm, *Resour. Conserv. Recycl.* 167:105395. <https://doi.org/10.1016/j.resconrec.2021.105395>.
- [16] Kargah-Ostadi, N., and S.M. Stoffels (2015). Framework for development and comprehensive comparison of empirical pavement performance models, *J. Transp. Eng.* 141:04015012. [https://doi.org/10.1061/\(ASCE\)TE.1943-5436.0000779](https://doi.org/10.1061/(ASCE)TE.1943-5436.0000779).
- [17] Ziari, H., J. Sobhani, J. Ayoubinejad, and T. Hartmann (2015). Prediction of IRI in short and long terms for flexible pavements: ANN and GMDH methods, *Int. J. Pavement Eng.* 17:776–788. <https://doi.org/10.1080/10298436.2015.1019498>.
- [18] Hoang, N.D. (2018). An Artificial Intelligence Method for Asphalt Pavement Pothole Detection Using Least Squares Support Vector Machine and Neural Network with Steerable Filter-Based Feature Extraction, *Adv. Civ. Eng.* 2018:1-12. <https://doi.org/10.1155/2018/7419058>.
- [19] S. Inkoom, J. Sobanjo, A. Barbu, X. Niu, Prediction of the crack condition of highway pavements using machine learning models, *Struct. Infrastruct. Eng.* 15 (2019) 940–953. <https://doi.org/10.1080/15732479.2019.1581230>.
- [20] Liu, G., F. Niu, and Z. Wu (2020). Life-cycle performance prediction for rigid runway pavement using artificial neural network, *Int. J. Pavement Eng.* 21:1806–1814. <https://doi.org/10.1080/10298436.2019.1567922>.
- [21] Abe, H., A. Tamai, J.J. Henry, and J. Wambold (2001). Measurement of Pavement Macrotexture with Circular Texture Meter, *Transp. Res. Rec. J. Transp. Res. Board.* 1764:201–209. <https://doi.org/10.3141/1764-21>.
- [22] Hu, L., D. Yun, Z. Liu, S. Du, Z. Zhang, and Y. Bao (2016). Effect of three-dimensional macrotexture characteristics on dynamic frictional coefficient of asphalt pavement surface, *Constr. Build. Mater.* 126:720–729. <https://doi.org/10.1016/j.conbuildmat.2016.09.088>.
- [23] Flintsch, G.W., E. de L. Izeppi, K.K. McGhee, and J.A. Roa (2009). Evaluation of International Friction Index Coefficients for Various Devices, *Transp. Res. Rec. J. Transp. Res. Board.* 2094:136–143. <https://doi.org/10.3141/2094-15>.
- [24] Al-Assi, M., and E. Kassem (2017). Evaluation of Adhesion and Hysteresis Friction of Rubber–Pavement System, *Appl. Sci.* 7:1029. <https://doi.org/10.3390/app7101029>.
- [25] Mataei, B., H. Zakeri, M. Zahedi, and F.M. Nejad (2016). Pavement Friction and Skid Resistance Measurement Methods: A Literature Review, *Open J. Civ. Eng.* 06:537–565. <https://doi.org/10.4236/ojce.2016.64046>.
- [26] Cossale, G., R. Elliott, and I. Widyatmoko (2013). The Importance of Road Surface Texture in Active Safety Design and Assessment, In *Road Saf. Simul. Int. Conf.*, 2013.
- [27] Cairney, P. (1997). *Skid resistance and crashes: A review of the literature*, Australian Road Research Board, Report No. 311.
- [28] Bitelli, G., A. Simone, F. Girardi, and C. Lantieri (2012). Laser Scanning on Road Pavements: A New Approach for Characterizing Surface Texture, *Sensors (Basel)* 12:9110–9128. <https://doi.org/10.3390/s120709110>.

- [29] Whitney, D., D.W. Fowler, and M. Rached (2012). *Use of Manufactured Sands for Concrete Pavement*, Texas Department of Transportation, Report No. FHWA/TX-13/0-6255-1.
- [30] Rezaei, A., and E. Masad (2013). Experimental-based model for predicting the skid resistance of asphalt pavements, *Int. J. Pavement Eng.* 14:24–35. <https://doi.org/10.1080/10298436.2011.643793>.
- [31] Flintsch, G.W., E. de León, K.K. McGhee, and I.L. Al-Qadi (2003). Pavement Surface Macrotecture Measurement and Applications, *Transp. Res. Rec. J. Transp. Res. Board* 1860:168–177. <https://doi.org/10.3141/1860-19>.
- [32] Komaragiri, S., A. Amirkhanian, and A. Bhasin (2020). Friction and Texture Retention of Concrete Pavements, *Transp. Res. Rec. J. Transp. Res. Board* 2674:457–465. <https://doi.org/10.1177/0361198120919397>.
- [33] Gardziejczyk, W., and P. Gierasimiuk (2018). Influence of texturing method on tyre/road noise of cement concrete pavement, *Int. J. Pavement Eng.* 19:1061–1076. <https://doi.org/10.1080/10298436.2016.1238699>.
- [34] Scofield, L. (2012). *Development and Implementation of the Next Generation Concrete Surface*, American Concrete Pavement Association.
- [35] Khasawneh, M.A. (2008). *The Development and Verification of a New Accelerated Polishing Machine*, Doctoral Dissertation, The University of Akron.
- [36] Choubane, B., C.R. Holzschuher, and S. Gokhale (2004). Precision of Locked-Wheel Testers for Measurement of Roadway Surface Friction Characteristics, *Transp. Res. Rec. J. Transp. Res. Board* 1869:145–151. <https://doi.org/10.3141/1869-17>.
- [37] Wang, W., X. Yan, H. Huang, X. Chu, and M. Abdel-Aty (2011). Design and verification of a laser based device for pavement macrotecture measurement, *Transp. Res. Part C Emerg. Technol.* 19:682–694. <https://doi.org/10.1016/j.trc.2010.12.001>.
- [38] Gui, R., X. Xu, D. Zhang, H. Lin, F. Pu, L. He, and M. Cao (2018). A Component Decomposition Model for 3D Laser Scanning Pavement Data Based on High-Pass Filtering and Sparse Analysis, *Sensors* 18:2294. <https://doi.org/10.3390/s18072294>.
- [39] Khasawneh, M.A., and M.A. Alsheyab (2020). Effect of nominal maximum aggregate size and aggregate gradation on the surface frictional properties of hot mix asphalt mixtures, *Constr. Build. Mater.* 244:118355. <https://doi.org/10.1016/j.conbuildmat.2020.118355>.
- [40] Prowell, B.D., and D.I. Hanson (2005). Evaluation of Circular Texture Meter for Measuring Surface Texture of Pavements, *Transp. Res. Rec. J. Transp. Res. Board* 1929:88–96. <https://doi.org/10.1177/0361198105192900111>.
- [41] China, S., and D.E. James (2012). Comparison of Laser-Based and Sand Patch Measurements of Pavement Surface Macrotecture, *J. Transp. Eng.* 138:176–181. [https://doi.org/10.1061/\(ASCE\)TE.1943-5436.0000315](https://doi.org/10.1061/(ASCE)TE.1943-5436.0000315).
- [42] Zhang, X., T. Liu, C. Liu, and Z. Chen (2014). Research on skid resistance of asphalt pavement based on three-dimensional laser-scanning technology and pressure-sensitive film, *Constr. Build. Mater.* 69:49–59. <https://doi.org/10.1016/j.conbuildmat.2014.07.015>.
- [43] Zhang, A., K.C.P. Wang, and S. Qiu (2018). Detecting Pavement Joints and Grooves with Improved 3D Shadow Modeling, *J. Comput. Civ. Eng.* 32:04018003. [https://doi.org/10.1061/\(ASCE\)CP.1943-5487.0000746](https://doi.org/10.1061/(ASCE)CP.1943-5487.0000746).

- [44] Dewey, G.R., A.C. Robords, B.T. Armour, and R. Muethel (2001). Aggregate Wear and Pavement Friction, in: *Transportation Res. Board Annual Meeting*, Washington DC, 7-11 January 2001, CD-ROM, 17 p.
- [45] Erukulla, S. (2011). *Refining a Laboratory Procedure to Characterize Change in Hot-Mix Asphalt Surface Friction*, Auburn University.
- [46] Crisman, B., G. Ossich, P. Bevilacqua, and R. Roberti (2019). Degradation Prediction Model for Friction of Road Pavements with Natural Aggregates and Steel Slags, *Appl. Sci.* 10:32. <https://doi.org/10.3390/app10010032>.
- [47] Cai, X., D. Wang, and J. Yu (2020). Evaluation of the Functional Performance of Paving Materials Based on the Driving Wheel Pavement Analyzer, *Appl. Sci.* 10:2410. <https://doi.org/10.3390/app10072410>.
- [48] Muethel, R.W. (1979). *The Michigan Department of Transportation Circular Wear Track - Results of Preliminary Aggregate Polishing Tests*, Michigan Department of Transportation, Report No. R-1098.
- [49] Vollor, T.W., and D.I. Hanson (2006). *Development of Laboratory Procedure for Measuring Friction of HMA Mixtures-Phase I*, Auburn University, NCAT Report 06-06.
- [50] Amir Khanian, A., S. Komaragiri, A. Algarni, M. Rung, D. Whitney, D. Fowler, A. Bhasin, M. Fetner, and A. Tuinukuafe (2019). *Friction and Texture Retention of Concrete Pavements*, University Transportation Center for Alabama, Report No. ALDOT 930-920.
- [51] McDaniel, R.S., A. Shah, and K.J. Kowalski (2018). *Development of Friction Performance Test for Compacted Asphalt Mixtures*, Report No. FHWA/IN/JTRP-2018/20, West Lafayette, IN: Purdue University. <https://doi.org/10.5703/1288284316865>.
- [52] Maryland Department of Transportation (2012). *Laboratory Method of Polishing Aggregates Using the Circular Track Polishing Machine*, Report No. MSMT 215.
- [53] Druta, C., L. Wang, and D.S. Lane (2014). *Evaluation of the MMLS3 for Accelerated Wearing of Asphalt Pavement Mixtures Containing Carbonate Aggregates*, Virginia Center for Transportation Innovation and Research, Final Report VCTIR 14-R17.
- [54] Wambold, J.C., C.E. Antle, J.J. Henry, and Z. Rado (1995). *International PIARC Experiment to Compare and Harmonize Texture and Skid Resistance Measurement*, Final Report, ISBN: 84-87825-96-6, Paris, France.
- [55] *PennDOT Bulletin 14*, Pub 34 (n.d.), Aggregate Producers, Supporting Information.
- [56] Louisiana Department of Transportation and Development (2016), *2016 Louisiana Standard Specifications for Roads and Bridges*, LA DOTD, Baton Rouge, LA.
- [57] Li, S., D. Harris, and T. Wells (2016). Surface texture and friction characteristics of diamond-ground concrete and asphalt pavements, *J. Traffic Transp. Eng. (English Ed.)* 3:475–482. <https://doi.org/10.1016/j.jtte.2016.08.001>.
- [58] Hastie, T., R. Tibshirani, and J. Friedman (2009). *The elements of statistical learning: Data mining, inference, and prediction, 2nd ed.*, Springer.
- [59] Wilamowski, B.M., and J.D. Irwin (2011). *Intelligent Systems, 2nd ed.*, CRC Press.
- [60] Young, B.A., A. Hall, L. Pilon, P. Gupta, and G. Sant (2019). Can the compressive strength of concrete be estimated from knowledge of the mixture proportions?: New insights from statistical analysis and machine learning methods, *Cem. Concr. Res.* 115:379–388. <https://doi.org/10.1016/j.cemconres.2018.09.006>.

- [61] Liang, R.Y. (2013). *Long Term Validation of an Accelerated Polishing Test Procedure for HMA Pavements*, Ohio Department of Transportation, Report No. FHWA/OH-2013/3.
- [62] Shojaeefard, M.H., M. Akbari, M. Tahani, and F. Farhani (2013). Sensitivity analysis of the artificial neural network outputs in friction stir lap joining of aluminum to brass, *Adv. Mater. Sci. Eng.* 2013(1). <https://doi.org/10.1155/2013/574914>.
- [63] Montañó, J.J., and A. Palmer (2003). Numeric sensitivity analysis applied to feedforward neural networks, *Neural Comput. Appl.* 12:119–125. <https://doi.org/10.1007/s00521-003-0377-9>.
- [64] Murad, M.M., and K.A. Abaza (2019). A closer look at the locked-wheel pavement friction data in the LTPP database for selected states, *Cogent Eng.* 6(1). <https://doi.org/10.1080/23311916.2019.1690214>.
- [65] Kowalski, K.J., R.S. McDaniel, and J. Olek (2016). Reclaimed Asphalt Pavement Limits to Meet Surface Frictional Requirements, *J. Mater. Civ. Eng.* 28:04015069. [https://doi.org/10.1061/\(ASCE\)MT.1943-5533.0001323](https://doi.org/10.1061/(ASCE)MT.1943-5533.0001323).
- [66] Ahammed, M., and S.L. Tighe (2009). Early-life, long-term, and seasonal variations in skid resistance in flexible and rigid pavements, *Transp. Res. Rec.* 2094:112–120. <https://doi.org/10.3141/2094-12>.
- [67] Li, S., K. Zhu, and S. Noureldin (2005). Considerations in developing a network pavement inventory friction test program for a state highway agency, *J. Test. Eval.* 33:287–294. <https://doi.org/10.1520/jte11885>.